POLITECNICO DI MILANO

POLO TERRITORIALE DI COMO

Scuola di Ingegneria Civile, Ambientale e Territoriale

Environmental and geomatic engineering master of science

Bayesian interpretation of gravity data with geological prior information

Supervisor: **Prof. Fernando Sansò**

Assistant supervisor: **Dr. Daniele Sampietro**

Master graduation thesis by:

Lorenzo Rossi

782476

Academic year 2012 - 2013

Acknowledgement

I wish to express my gratitude to prof. Fernando Sansò for his encouragement, thoughtful guidance and willingness in the developing of my thesis work. I would also like to thank the co-tutor Dr. Daniele Sampietro, whose suggestions that have improved the quality of my final thesis work. I would also thank both for the opportunities and the learning experiences proposed during my studiy that allowed me to grow professionally and personally.

I would to thank also my family for all the support and the motivation received during this years. In particular my parents for their closeness to me and all their teaching, despite all the difficulties encountered.

A special thank to Greta for every moment shared in the last years together.

Ringraziamenti

Vorrei esprimere la mia gratitudine al prof. Fernando Sansò, per il suo incoraggiamento, guida e disponibilità nello sviluppo del mio lavoro di tesi. Vorrei anche ringraziare il correlatore Dr. Daniele Sampietro per i suoi suggerimenti che hanno migliorato la qualità finale del mio elaborato di tesi. Inoltre vorrei ringraziare entrambi per le opportunità e le esperienze di apprendimento che mi hanno proposto durante il mio percorso studi che mi hanno permesso di cresecere professionalmente e personalmente.

Vorrei ringraziare anche la mia famiglia, per il supporto e le motivazioni ricevute durante questi anni. In particolare i miei genitori per la loro vicinanza ed insegnamento, nonostante tutte le difficoltà incontrate.

Da ultimo, un ringraziamento speciale a Greta per tutti i momenti condivisi insieme in questi anni.

Contents

List of Figures

Abstract

It is well known that the gravimetric inverse problem, namely the reconstruction of the Earth mass density distribution from the observation of the gravitational field, is generally ill-posed. For this reason its solution requires some restrictive hypotheses and strong numerical regularization. These constrains rarely take into account the specific local characteristics of the area under study, thus leading to solutions that are theoretically and physically admissible but that could be far from the actual mass density distribution. To mitigate this problem, the inversion method could be driven by some qualitative geological information that is usually available.

In this work, a Bayesian approach to estimate a mass density distribution from gravity data coupled with geological information is presented. It requires to model the masses in voxels, each of them characterized by two random variables: one is a discrete label defining the type of material, the other is a continuous variable defining the mass density. The a-priori geological information can be easily translated in terms of this model, providing for each class of material the mean density and the corresponding variability and for each voxel the a-priori most probable label. Basically the method consists of a simulated annealing aided by a Gibbs sampler to update the labels of the a-priori model in order to maximize the posterior probability, introducing some proximity constrains between labels of adjacent voxels.

The proposed Bayesian method is here tested on simulated scenarios, comparing it with classical solutions based on a regularized least-squares adjustment and showing its capability of correcting possible inconsistencies between the a-priori geological model and the gravity observations.

Riassunto esteso

Sommario

È ben noto che il problema gravimetrico inverso, cioè la ricostruzione della distribuzione della massa all'interno della Terra partendo dall'osservazione del campo gravitazionale, è generalmente mal condizionato. Per questo motivo la sua soluzione richiede alcune ipotesi restrittive ed una forte regolarizzazione numerica. Questi vincoli, raramente, tengono conto delle caratteristiche specifiche della zona in esame, determinando in tal modo soluzioni che sono teoricamente e fisicamente ammissibili, ma che potrebbero essere molto lontane dall'effettiva distribuzione di densità della massa. Per attenuare questo problema, il metodo di inversione dovrebbe essere guidato da informazioni geologiche, di natura qualitativa.

In questo lavoro, viene presentato un approccio Bayesiano per stimare la distribuzione di densità a partire da osservazioni di gravità accoppiate con informazioni geologiche. La massa dell'area di studio viene modellizata con l'utilizzo di voxel, ognuno caratterizzato da due variabili casuali: la prima è un'etichetta discreta che caratterizza il tipo di materiale, l'altra una variabile continua che definisce la densità. L'informazione geologica nota a priori può essere facilmente tradotta in questi termini, fornendo per ciascuna classe di materiale litologico la densità media e la relativa variabilità, oltre all'etichetta più probabile per ciascun voxel desumibile dalla conoscenza a priori. Fondamentalmente, il metodo consiste nell'applicazione di un *simulated annealing* affiancato dal *Gibbs sampler* per aggiornare le etichette del modello a priori la probabilità a posteriori, con l'introduzione di alcuni vincoli di prossimità tra le etichette di voxel adiacenti.

Il metodo Bayesiano proposto viene testato su scenari simulati, confrontato con soluzioni classiche basate su compensazione ai minimi quadrati regolarizzata e mostra la sua capacità di correggere eventuali incoerenze tra il modello geologico a priori e le osservazioni di gravità.

Introduzione

L'Interpretazione di una serie di osservazioni del campo di gravità sulla superficie terrestre in termini di anomalie di densità è un problema scientificamente molto interessante e particolarmente rilevante nell'ambito delle prospezioni geofisiche, ma presenta il grande problema dell'indeterminatezza nella soluzione. Quindi, qualunque tecnica di interpretazione gravimetrica deve essere necessariamente combinata con informazioni note a priori, come quelle derivanti da vincoli puramente geofisici

o matematici oppure da indagini svolte con altri metodi di prospezione geofisica. Nel primo caso, ad esempio, può essere adottato un modello a due strati (Sampietro and Sansó, 2012) oppure si può fissare il contrasto di densità tra i corpi geologici (Dumrongchai, 2007), mentre nel secondo, ad esempio, si possono dedurre dei vincoli da prospezioni magnetiche, si veda Abt et al. (2012), o sismiche, come descritto da Barzaghi and Sansò (1998) o Darbyshire et al. (2000).

Qualunque sia il metodo usato, le applicazioni pratiche sfruttano sempre un modello geologico del sottosuolo e spesso soluzioni semplici del tipo *trial and error* vengono implementate manualmente da un esperto del settore, con l'obiettivo di non modificare troppo il punto di partenza e cercando di rendere il più simile possibile l'anomalia di gravità modellizzata a quella osservata.

La presente tesi si pone lo scopo di formalizzare le operazioni iterative appena descritte mediante l'utilizzo di un approccio statistico Bayesiano. L'uso della statistica Bayesiana ha una lunga storia di applicazione nelle prospezioni geofisiche; si vedano per esempio Tarantola and Valette (1982), Bosch (1999), Tarantola (2002) o Mosegaard and Tarantola (2002), solo per citarne alcuni. Il punto fondamentale risiede nella scelta delle variabili specifiche del problema e nella formalizzazione della loro distribuzione di probabilità a priori. Durante il processo di stima del MAP (Massimo a Posteriori) delle distribuzioni di probabilità a posteriori si devono trattare variabili in parte discrete ed in parte continue. La soluzione ricorre all'applicazione di un *Gibbs sampler* combinato con un *simulated annealing* (Sansò et al., 2011), come descritto ampiamente in letteratura; è opportuno citare il lavoro di Geman and Geman (1984), dove l'approccio Bayesiano è applicato al campo dell'analisi di immagine.

Tuttavia, è necessario sottolineare che, mentre l'analisi delle immagini si occupa solo di osservazioni "locali", cioè dipendenti unicamente dal pixel da aggiornare, al contrario, in questo caso, una variazione di densità in qualsiasi punto dello volume preso in esame influenzerà ogni osservazione dell'anomalia gravitazionali, indipendentemente dalla sua posizione. Questo comporta piccole variazioni alle tecniche fin'ora menzionate.

Formalizzazione del problema

Alla base del metodo di soluzione vi è il teorema di Bayes, di seguito espresso nella sua forma consueta (Bayes, 1984; Box and Tiao, 2011):

$$P(\mathbf{x}|\mathbf{y}) \propto \mathcal{L}(\mathbf{y}|\mathbf{x})\, P(\mathbf{x}) \tag{1}$$

dove $\mathbf{y}$ è un vettore di osservabili, mentre $\mathbf{x}$ è un vettore di parametri del corpo geologico. Il corpo B è diviso in voxel V_i, con indice $i = 1, 2, ..., N$; ad ogni voxel sono associati due parametri (ρ_i, L_i) dove ρ_i rappresenta la densità di massa considerata costante nel voxel e L_i è un'etichetta che descrive il tipo litologico, quale acqua, sedimenti, sale, roccia di un dato tipo, ecc, presente all'interno dello spazio delimitato da V_i. L'insieme dei materiali geologici viene assegnato a priori da un archivio, sulla base delle caratteristiche specifiche del luogo in esame. Concludendo, ρ_i risulta essere una variabile continua e L_i discreta. Infatti può assumere solo uno degli M interi che indicano i vari materiali selezionati.

È fondamentale il modo in cui viene descritta l'informazione a priori, cioè la forma della distribuzione di probabilità $P(\mathbf{x}) = P(L_1, \rho_1; L_2, \rho_2; ...; L_N, \rho_N)$. Si assume che:

$$P(\mathbf{x}) = \prod_i P(\rho_i|L_i) \cdot P(L_1, L_2, ..., L_N) \tag{2}$$

e successivamente che una volta che un'etichetta $L_i = \ell$ è stata scelta per V_i, la corrispondente densità segue la legge $P(\rho_i|L_i)$, che nel caso in esame è semplicemente una distribuzione di probabilità normale:

$$P(\rho_i|L_i) \sim \mathcal{N}\left(\overline{\rho}_\ell, \sigma_\ell^2\right) \tag{3}$$

con la media $\overline{\rho}_\ell$ e la varianza σ_ℓ^2 fornite da tabelle geologiche. A questo riguardo, una corposa raccolta di dati relativi alle proprietà delle rocce può essere trovata per esempio in Christensen and Mooney (1995). Per la distribuzione di probabilità a priori $P(\mathbf{L}) \equiv P(L_1, L_2, ..., L_N)$ si assume di avere una distribuzione di Gibbs (Azencott, 1988):

$$P(\mathbf{L}) = e^{-\mathcal{E}(\mathbf{L})}, \tag{4}$$

dove l'energia $\mathcal{E}(\mathbf{L})$ dipende solamente dai valori ℓ_i^o di L_i forniti con il modello a priori, così come dalle cliques di ordine due, che rappresentano il fatto che l'etichetta L_i sia probabilmente simile a quella dei voxel vicini, secondo la seguente regola:

$$P(L_i = \ell|\mathbf{L}_{\Delta i}) \propto e^{-\gamma s^2\left(L_i, \ell_i^o\right) - \lambda \sum_{j \in \Delta_i} q^2(L_i, L_j)} \tag{5}$$

dove γ, λ sono parametri da regolare, e

$$s^2(L_i, \ell_i^o) = \begin{cases} 0 & \text{if } L_i = \ell_i^o \\ \alpha_k & \text{if } L_i = k \neq \ell_i^o \end{cases} \tag{6}$$

$$q^2(L_i, L_j) = \begin{cases} a & \text{if } L_i = L_j \\ a_j & \text{if } L_i \neq L_j \end{cases}, \tag{7}$$

con $V_j \in \Delta_i$ essendo Δ_i un intorno del voxel V_i.

Si noti che tarando α_k e a, a_j si può creare una gerarchia di valori più probabili per L_i, così da ottenere una tabella di prossimità tra unità geologiche note a priori. Per esempio, supponendo di avere tre litotipi differenti, $\ell = \{1, 2, 3\}$, ed una tabella di prossimità tipo quella rappresentata in figura 1, ne deriva la seguente definizione:

$$s^2 = \begin{cases} 0 & \text{if } L_i = \ell_i^o \\ \alpha & \text{if } L_i \text{ is a } 1^{st} \text{ neighbour of } \ell_i^o \\ \beta & \text{if } L_i \text{ is a } 2^{nd} \text{ neighbour of } \ell_i^o \end{cases}, \tag{8}$$

$$q_j^2 = \begin{cases} a & \text{if } L_i = L_j \\ b & \text{if } L_i \text{ is a } 1^{st} \text{ neighbour of } L_j \\ c & \text{if } L_i \text{ is a } 2^{nd} \text{ neighbour of } L_j \end{cases} \tag{9}$$

dove $\beta > \alpha > 0$ e $c > b > a$.

	1	2	3
1	X	X	
2	X	X	X
3		X	X

Figura 1: Esempio di tabella di prossimità. La classe geologica 1 può essere vicino a 2, ma non alla 3

Due osservazioni importanti sono, in ordine: la prima che $\mathbf{L}$, con una distribuzione a priori $P(\mathbf{L})$, è rappresentata da un *Markov random field* (MRF, cfr. Rozanov 1982), mentre la seconda è che il risultato finale dell'ottimizzazione dipende fortemente dai valori scelti per le varie costanti, che nel caso specifico necessitano di essere tarate a mano dall'operatore.

Come sempre per un MRF, le caratteristiche, cioè le distribuzioni di probabilità condizionate (5), definiscono una distribuzione $P(\mathbf{L})$ del tipo:

$$\log P(\mathbf{L}) \propto -\gamma \sum_i s^2(L_i, \ell_{oi}) - \lambda \sum_i \sum_{j \in \Delta_i} q^2(L_i, L_j). \tag{10}$$

Concludendo il logaritmo della distribuzione di probabilità a posteriori (1) può essere scritto come:

$$\begin{aligned} L(\mathbf{x}) = L(\boldsymbol{\rho},\ \mathbf{L}\ ) = \log P(\mathbf{x}|\mathbf{y}) = -\frac{1}{2}(\boldsymbol{\Delta g} - A\boldsymbol{\rho})^T \boldsymbol{C}_{\boldsymbol{\Delta g}}^{-\mathbf{1}}(\boldsymbol{\Delta g} - A\boldsymbol{\rho}) + \\ -\frac{1}{2}(\boldsymbol{\rho} - \overline{\boldsymbol{\rho}})^T \boldsymbol{C}_{\boldsymbol{\rho}}^{-\mathbf{1}}(\boldsymbol{\rho} - \overline{\boldsymbol{\rho}}) - \frac{1}{2}\gamma \sum_i \mathbf{s}^2(\ell_i, \ell_i^o) - \lambda \sum_i \sum_{j \in \Delta_i} \mathbf{q}^2(\ell_i, \ell_j) \end{aligned} \tag{11}$$

dove si ricorda che $\boldsymbol{\Delta g}$ è il vettore delle anomalie di gravità osservate, $\boldsymbol{C}_{\boldsymbol{\Delta g}}$ la matrice di covarianza del loro errore che si assume essere diagonale, A è l'operatore che definisce il forward per passare dalle densità alle anomalie di gravità, $\boldsymbol{\rho}$ and $\overline{\boldsymbol{\rho}}$ i vettori composti da ρ_i e $\overline{\rho}_i = \overline{\rho}(\ell_i)$, $\boldsymbol{C}_{\boldsymbol{\rho}}$ la corrispondente matrice di covarianza e s^2, q^2 dati dalle equazioni 6 e 7. Questa è la funzione obiettivo da massimizzare rispetto a ρ_i e L_i.

Algoritmo di ottimizzazione

Il fatto che la metà delle variabili siano discrete rende difficile la massimizzazione dell'equazione 11, come noto da altri problemi importanti trattati in geodesia, come il fissaggio dell'ambiguità di fase iniziale nel GNSS (De Lacy et al., 2002). L'idea mutuata dalle tecniche di analisi di immagine è di applicare il *Gibbs sampler*, concatenato con il *simulated annealing*. Per far si che questa tecnica possa essere applicata ad entrambe le variabili (ρ_i, L_i), funzioni del voxel V_i, si è deciso di semplificare il problema, considerando discreta anche ρ_i. In pratica la distribuzione normale di probabilità (equazione 3) viene sostituita da una distribuzione discreta

di cinque valori presi rispettivamente in corrispondenza della media $\overline{\rho}$, e di $\overline{\rho} \pm \sigma_\rho$, $\overline{\rho} \pm 2\sigma_\rho$. Chiaramente, ad ogni valore deve essere assegnata un opportuno valore di probabilità, secondo la distribuzione normale. Quindi, si può applicare il *Gibbs sampler* campionando una coppia (ρ_i, L_i) alla volta, mantenendo fissati tutti gli altri valori e seguendo un semplice algoritmo di aggiornamento. La probabilità del campionamento può essere calcolata dall'equazione 11 facendo assumere a ρ_i i suoi cinque valori e scegliendo ℓ_i tra i valori $1, 2, ..., M$ definiti per il volume oggetto di studio; in questo modo si può costruire una tabella di $5M$ nodi, associati alla propria probabilità. Una volta che un'iterazione con il *Gibbs sampler* è stata eseguita sull'insieme dei voxel, la probabilità di $\mathbf{x}$ viene cambiata introducendo un parametro T, chiamato, in analogia con l'applicazione meccanica, "temperatura":

$$P_T(\mathbf{x}) \propto e^{\frac{1}{T}\log P(\mathbf{x})} \tag{12}$$

dove T viene lentamente ridotto del 5% ad ogni passo. Infine, partendo da una temperatura T molto elevata si ottiene una sequenza di campionamenti convergenti al punto $\overline{\mathbf{x}}$ dove $\log P(\mathbf{x})$ raggiunge il suo massimo (Azencott, 1988). È opportuno notare che durante il processo la probabilità condizionata di una coppia (ρ_i, L_i) campionata può essere calcolata, cosicché lungo la sequenza iterativa, questa tenda a stabilizzarsi sul valore più alto possibile nella maggior parte dei voxel.

Test numerici

Per poter accertare l'effettiva funzionalità dell'approccio Bayesiano trattato, in grado di integrare anche le informazioni geologiche del tutto qualitative, sono stati effettuati una serie di esperimenti. I test consistono nella stima della distribuzione di densità di due modelli sintetici tridimensionali a partire dal campo gravitazionale da essi generato. In particolare il primo simula la stima della batimetria, mentre il secondo consiste nel ricavare la forma di un duomo salino. Nel primo esempio vengono considerate solo due etichette: acqua e roccia, definite rispettivamente da $\rho_w = 1000\ kg\,m^{-3}$, $\sigma_w = 30\ kg\,m^{-3}$ e $\rho_b = 2900\ kg\,m^{-3}$, $\sigma_b = 80\ kg\,m^{-3}$. Invece, nel secondo test, relativo al duomo salino, si sono considerate tre unità geologiche: sedimenti ($\rho_s = 2200\ kg\,m^{-3}$, $\sigma_s = 40\ kg\,m^{-3}$), sale ($\rho_d = 2000\ kg\,m^{-3}$, $\sigma_d = 20\ kg\,m^{-3}$) e roccia ($\rho_b = 2900\ kg\,m^{-3}$, $\sigma_b = 80\ kg\,m^{-3}$).

In entrambi i casi l'area di interesse è un quadrato di lato 30 *km* e la profondità di investigazione di 5 *km*. Inoltre il modello sintetico è considerato costante lungo una direzione planimetrica. Una sezione verticale significativa dei modelli è rappresentata nelle figure 2(a) and 3(a). Il volume è modellato con l'utilizzo di 1200 prismi rettangolari, ciascuno di dimensioni 1.5 *km (x)* × 5.0 *km (y)* × 0.5 *km (z)*. A partire da questi modelli il relativo campo gravitazionale viene calcolato. In particolare si usa l'equazione di Nagy per il prisma (Nagy, 1966; Nagy et al., 2000) in uno scenario privo di *noise*. Le osservazione sono generate su di una griglia regolare ad una quota di 500 *m* e con risoluzione spaziale di 5 *km*, così da simulare un volo aerogravimetrico.

Il modello geologico è simulato introducendo piccole modifiche in quello di riferimento, come mostrato nelle figure 2(b) and 3(b). I due parametri λ e γ dell'equazione

11 sono stati rispettivamente impostati empiricamente ai valori di 0.833 e 0.733. Infine, i valori iniziali delle etichette sono inizializzati in maniera casuale, estraendo da una distribuzione uniforme (i.e. campionamento con la temperatura impostata ad infinito nel *simulated annealing*).

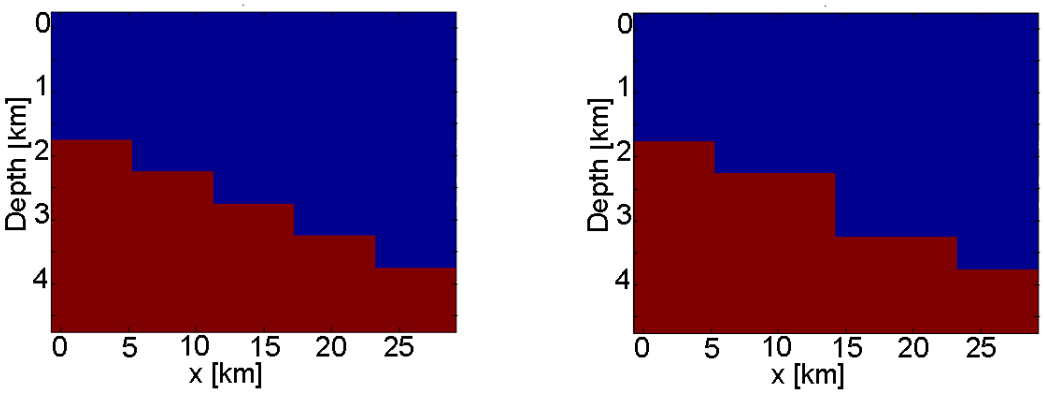

(a) (b)

Figura 2: Sezione verticale del modello di batimetria vero (a) e geologico (b), dove in blu è rappresentata l'acqua ed in rosso la roccia

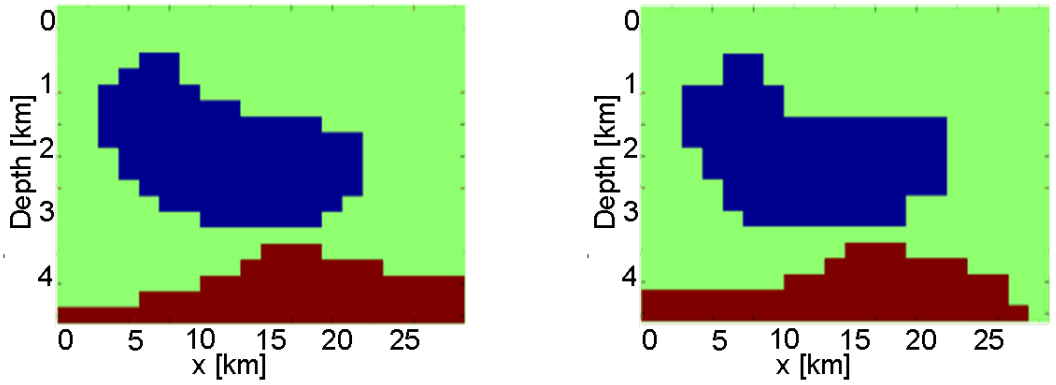

(a) (b)

Figura 3: Sezione verticale del modello di batimetria vero (a) e geologico (b), dove in blu sono rappresentati i sedimenti, in verde il sale ed in rosso la roccia

La soluzione finale è ricavata in circa 5000 iterazioni e 4 ore di calcolo utilizzando un comune personal computer. Una sezione del modello risultante è visibile in figura 4 e chiaramente mostra come l'errore nel modello geologico a priori sia propriamente corretto nel caso della batimetria (86% delle etichette e densità sbagliate sono correttamente stimate), ma solo parzialmente nel caso del duomo salino (70% delle etichette e densità sbagliate sono correttamente stimate).

Infine, è interessante comparare i risultati ottenuti con quelli di una soluzione ai minimi quadrati, dove la regolarizzazione è fatta sulla base del modello geologico.

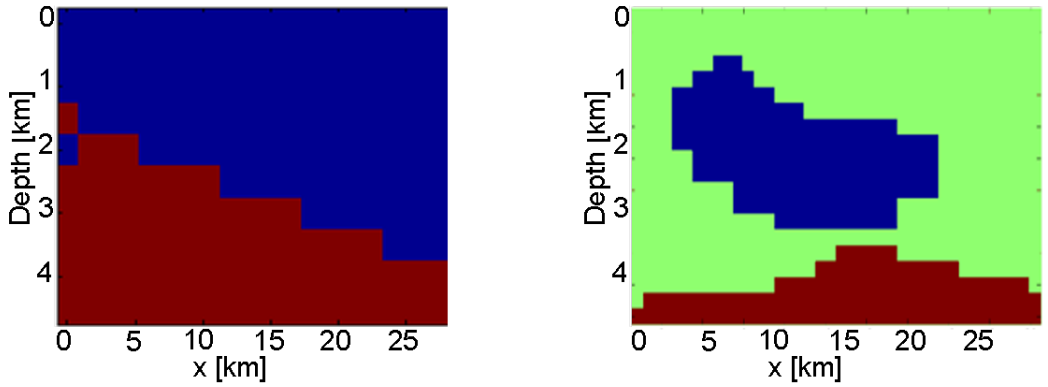

Figura 4: Risultato dell'inversione Bayesiana derivata dalle osservazioni simulate (sezione verticale a $y = 10\ km$)

Come si vede dalla figura 5 non si è in grado di modificare le etichette dei voxel, ma la compensazione ai minimi quadrati si limita solamente a interpolare le osservazioni, cambiando le densità sulla base delle ipotesi a priori ed evidentemente la soluzione non è in grado di identificare possibili errori nel modello a priori.

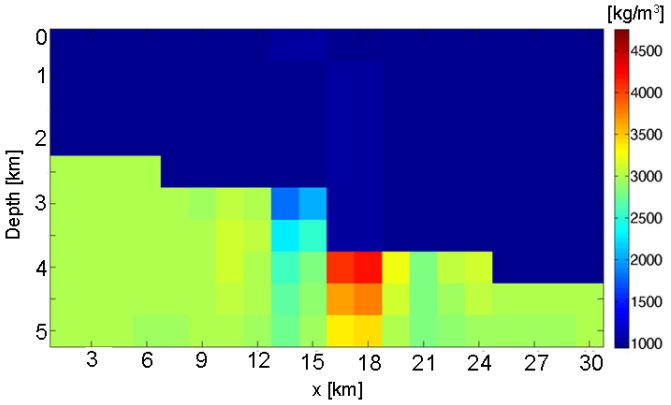

Figura 5: Stima delle densità tramite inversione ai minimi quadrati regolarizzata

Conclusioni e sviluppi futuri

Nell'elaborato di tesi viene presentato un approccio Bayesiano all'inversione di dati gravimetrici accoppiati con un modello geologico noto. Il metodo funziona correttamente nei semplici esempi trattati, migliorando la qualità della soluzione se comparata con quella ottenuta attraverso tecniche di inversione tradizionale. Allo stato attuale i maggiori due fattori limitanti sono il tempo necessario per il calcolo e la scelta di parametri e costanti nella formulazione della distribuzione di probabilità a priori. Inoltre nella soluzione giocano un elevato numero di incognite, che determinano un'alta variabilità ed instabilità della soluzione.

In futuro l'algoritmo necessiterà un'ottimizzazione in modo da poter aumentare la risoluzione del modello così da diventare utile per trattare casi reali. Questo passo però, implica un enorme incremento del numero di variabili, che passano da qualche

migliaia a qualche milione, provocando effetti deleteri sul tempo di calcolo. Inoltre, un'ulteriore sviluppo necessario nell'implementazione dell'invertitore gravimetrico Bayesiano è quello di rendere semi-automatica la definizione di pesi e parametri, così da limitare al massimo le decisione dell'utente nel processo risolutivo.

Chapter 1

Gravity surveying

The measurement of gravitational field of the Earth is a very interesting scientific matter, especially for its implications in geophysical exploration. In fact, gravity surveying is widely used in Earth's science for regional geological studies, as well as for oil and hydrocarbon research, because of its accuracy, spatial resolution and costs - benefits ratio.

The fundamental idea of gravity field interpretation is to detect variations of density in the subsurface from the so-called gravity anomalies, i.e. the difference between the observed gravity and the one generated by a proper reference "normal" model. This problem is usually called inverse gravimetric problem.

In the current chapter it is provided a basic description of theoretical aspects of the Terrestrial gravity field, the measurement equipment that can be used and the preprocessing of data to isolate the gravity anomalies. For further details on these topics the reader can refer to Heiskanen and Moritz (1967), Hofmann-Wellenhof and Moritz (2006), Fedi and Rapolla (1993), or Blackely (1996).

1.1 Gravity constituent

The gravimetric signal of a mass is described by Newton's law of universal gravitation, which states that the force of attraction between two generic point masses m_P and m_Q can be describe as follows:

$$\mathbf{F}_{QP} = -Gm_P m_Q \frac{\mathbf{r}_{QP}}{|\mathbf{r}_{QP}|^3} \tag{1.1}$$

where $\mathbf{r}_{QP}$ is the vector between point P and Q (see figure 1.1) and G is the Gravitational Constant equal to $6.67384 \cdot 10^{-11} m^3 kg^{-1} s^{-2}$. The acceleration exerted by the Gravitational force $\mathbf{F}_{QP}$ on the mass m_P can be derived introducing Newton's Second Law of motion. Equation 1.1 becomes:

$$\mathbf{F}_{QP} = m_P \, \mathbf{g}\,(P) = m_P \left[-Gm_Q \frac{\mathbf{r}_{QP}}{|\mathbf{r}_{QP}|^3} \right] \tag{1.2}$$

Dividing by m_P it is possible to obtain the acceleration $\mathbf{g_P}$, called gravity acceleration. This is a vectorial conservative field and its name is gravitational vectorial field.

In order to study the Terrestrial gravity field some approximations must be removed. Mass P cannot be considered a point mass. Density $\rho(\mathbf{r_Q})$ and volume v_Q of the attractive body must be introduced. The total mass is the integral all over the volume of the density (see figure 1.2) and equation 1.2 turns in equation 1.3.

$$\mathbf{g}_P(\mathbf{r}_P) = -G\int_{v_Q}\rho(\mathbf{r}_Q)\frac{(\mathbf{r}_P-\mathbf{r}_Q)}{|(\mathbf{r}_P-\mathbf{r}_Q)|^3}dv_Q \tag{1.3}$$

where $\mathbf{r}_Q \in v_Q$ and $\mathbf{r}_P$ is the position of the point where the field is observed, outside the volume of the body. The consequence of this result is that every point of the body affects the gravity observed in every generic point P.

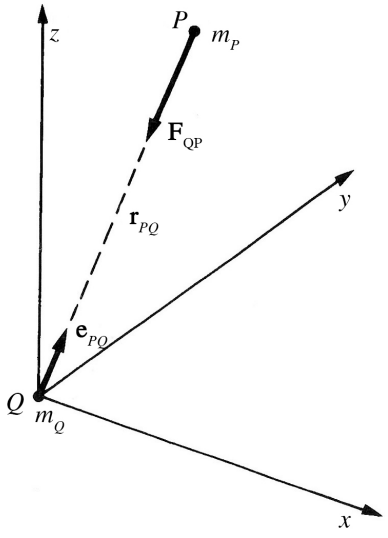

Figure 1.1: Gravitational attraction between two point masses (Fedi and Rapolla, 1993)

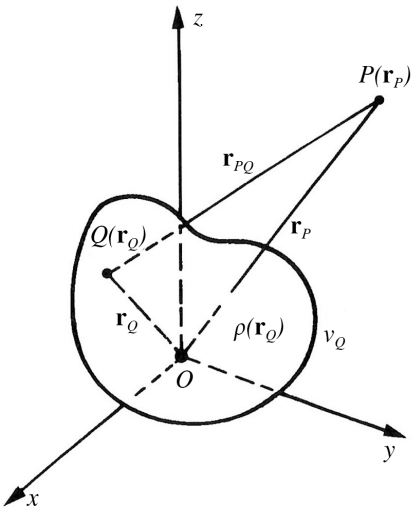

Figure 1.2: Gravitational field due to a generic mass distribution (Fedi and Rapolla, 1993)

In the International System of Units gravity field should be measured in ms^{-2}, but nowadays the *c.g.s.* system is still used in gravity practice. So the basic units is cms^{-2}, called *Gal*, in honour of the Italian scientist Galileo who makes the first measurement of the Earth's gravity acceleration. Often the sub-multiples *mGal* and μGal are used based on the application (gravimetry or microgravimetry).

One fundamental concept, in the theory of gravitation, is the gravitational potential $V(P)$; this is by definition a scalar function such that (Todhunter, 1873; Heiskanen and Moritz, 1967)

$$\mathbf{g}(P) = \nabla V(P) \tag{1.4}$$

where $\nabla = \mathbf{e}_x\frac{\partial}{\partial x} + \mathbf{e}_y\frac{\partial}{\partial y} + \mathbf{e}_z\frac{\partial}{\partial z}$ is the gradient operator represented in Cartesian coordinates; $\mathbf{e}_x$, $\mathbf{e}_y$, $\mathbf{e}_z$ are unit vectors parallels to x, y and z axes respectively. Since for a generic point mass M holds

$$\mathbf{g}(P) = -GM\frac{\mathbf{r}_{QP}}{|\mathbf{r}_{QP}|^3} = \nabla_P\left(\frac{GM}{|\mathbf{r}_{QP}|}\right) \tag{1.5}$$

it is always possible to describe the gravitational field in terms of its potential, as it can be directly verified. By using 1.5 in 1.3 and by given suitable regularity condition on ρ (e.g. it has to be measurable and bounded) and on the domain v_Q (e.g. the volume of Q must be finite) it's possible to write

$$\mathbf{g}_P = G \int_{v_Q} \left(\nabla_P \frac{1}{|\mathbf{r}_{QP}|} \right) \rho(Q)\, dv_Q = \nabla_P \left(G \int_{v_Q} \frac{\rho(Q)}{|\mathbf{r}_{QP}|} \right) dv_Q \tag{1.6}$$

In order to study the Earth's gravitational acceleration its motion should be properly considered. In fact the Earth has a rotational motion around the Sun and a revolution motion around its axis. Recalling Coriolis theorem as in equation 1.7 the gravity attraction measured from a point integral with the Earth can be fully explained (Sansò and Sideris, 2012).

$$\mathbf{a}' = \mathbf{a} + \boldsymbol{\omega} \times (\boldsymbol{\omega} \times \mathbf{r}) + 2\boldsymbol{\omega} \times \mathbf{v} \tag{1.7}$$

where $\boldsymbol{\omega}$ and $\mathbf{a}'$ are respectively the angular velocity of the Earth and the acceleration of the point in an inertial reference frame from which the Earth's one is observed, while $\mathbf{a}$, $\mathbf{v}$, and $\mathbf{r}$ are respectively the acceleration, the velocity and the position of the point in the Terrestrial frame. Since the point of measurement has no velocity with respect to the Earth, i.e. $\mathbf{v} = 0$, the last term of equation 1.7 is null. Thus the gravity field observed from a generic point on the Earth's surface become:

$$\mathbf{g} = \mathbf{g}' - \boldsymbol{\omega} \times (\boldsymbol{\omega} \times \mathbf{r}) \tag{1.8}$$

where $\mathbf{g}'$ is the gravity acceleration and could be computed introducing the volume and the density of the Earth in equation 1.3. Furthermore, it's important to remember that there are also other small factor that affect the gravity field, like lunar and solar attraction, that should be properly modelled and removed.

As a first approximation the Earth can be considered an oblate ellipsoid of revolution. In the same way a first approximation of the Earth gravity field can be considered as the sum of the known centrifugal field and of gravitational field that has the reference ellipsoid as equipotential surface and that is generated by a mass equal to the one of the Earth (Moritz, 1990). The modulus of this theoretical field g_T vary with the latitude and its general formulation is expressed in equation 1.9, derived with the integration and development of equation 1.8. The final expression contains also a term related to the height above the reference ellipsoid h (Hofmann-Wellenhof and Moritz, 2006). In this way the computation of free-air correction is already included as will be explained in paragraph 1.3.

$$g_T(P) = g_0 \left(1 + \alpha_1 \sin^2 \varphi_P + \alpha_2 \sin^2 2\varphi_P\right) - \left(\beta_0 - \beta_1 \sin^2 \varphi_P\right) h_P + c_0 h_P^2 \tag{1.9}$$

where $g_T(P)$ is expressed in Gal and h must be inserted in km. The values of the others parameters in the formula using the Internetional ellipsoid are (Hofmann-

Wellenhof and Moritz, 2006):

$$\begin{aligned} g_0 &= 978.0490 \\ \alpha_1 &= 0.0052884 \\ \alpha_2 &= 0.0000059 \\ \beta_1 &= 0.30877 \\ \beta_2 &= 0.00045 \\ c_0 &= 0.000072 \end{aligned}$$

An anomalous mass body generate a deviation of the measured gravity from this theoretical value, that can be computed simply by equation 1.10:

$$\Delta g^o = g^o(P) - g_T(P) \tag{1.10}$$

1.2 Data preprocessing

Section 1.1 give a generic description of the measured gravity signal, but in order to obtain a useful observable some other phenomena must be considered. It should be noted that the reduction for the normal field is a fundamental task in gravity interpretation. In fact, as shown in figure 1.3 the signal of interest for geophysical

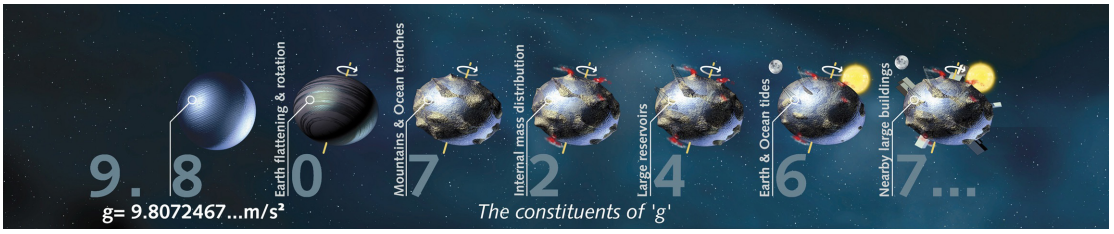

Figure 1.3: Main constituent of terrestrial gravity field (ESA)

studies is in general more than 4 order of magnitude smaller than the total observed gravity field.
The gravity signal can be thought as the sum of the following effects:

- attraction of the reference ellipsoid;
- effect of elevation above sea level (free-air);
- effect of normal masses above sea level (Bouger and terrain);
- time-dependent variation (tidal);
- effect of masses that support topographic load (isostatic);
- effect of crust and upper mantle density variation ("geology").

The last point of the list is what gravity prospecting is interest in. Therefore, to isolate that portion of the signal, called gravity anomaly, all the other listed effects must be removed, during the signal preprocessing. Conventionally, the average crustal density is assumed to be 2670 kgm^{-3}, so the exploration look for density contrast respect to this value. The basic concept of the standard preprocessing procedure is shown in figure 1.5. The main steps of the preprocessing can be summarized in the following steps:

1. remove normal gravity, i.e. the gravity generated from the reference ellipsoid, from the observed gravity signal, using the first terms of equation 1.9; i.e.:

$$\Delta g_N^o = g^o - g_N = g^o - g_T(P) = g^o - g_0\left(1 + \alpha_1 \sin^2 \varphi_P + \alpha_2 \sin^2 2\varphi_P\right)$$

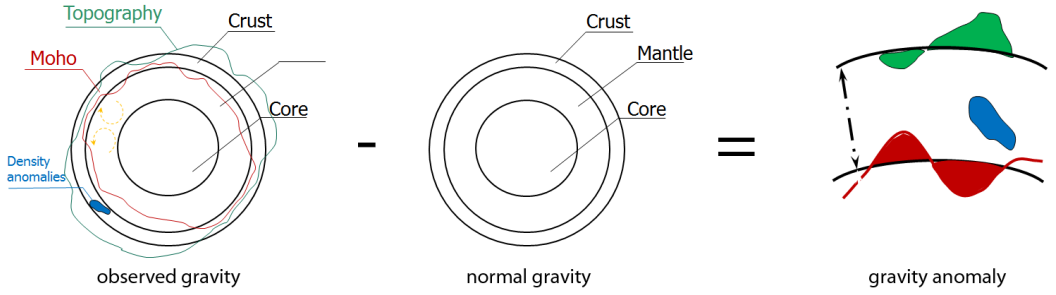

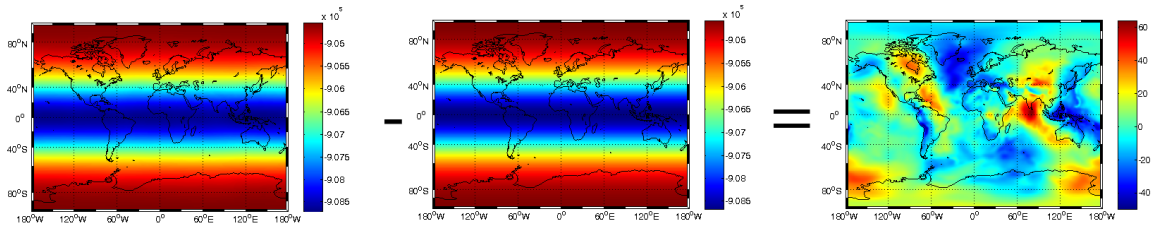

Figure 1.4: Gravity anomalies isolation

2. apply the so called free-air correction. It is necessary in order to consider the elevation of the point respect to the geoid. The classical formulation of the free-air correction is $F.A. = 0.3086H$ (Hofmann-Wellenhof and Moritz, 2006). This term is already considered in equation 1.9 thus the so-called free-air gravity anomaly can be expressed as:

$$\Delta g_{FA}^o = \Delta g_N^o + F.A. = \Delta g_N^o + 0.3086H$$

or, including the free-air correction in the normal gravity and recalling equation 1.9:

$$\Delta g_{FA}^o = g^o - g_T$$

3. remove the effect of the topographic masses applying the terrain correction and thus generating the Bouger gravity anomaly Δg^o that is suitable for the interpretation. The most simple way to carry out this operation is to remove a Bouger plate with standard density $\rho = 2667 kgm^{-3}$ from the observation. Hence the final formulation of the correction become $A_B = 0.1119H\,[mGal]$. The masses surplus of this rough topography approximation is removed trough the Terrain correction or residual terrain correction.

The final expression of the Bouger gravity anomaly is derived as follows:

$$\Delta g_B^o = g^o(P) - g_N(P) + F.A.(P) - T.C.(P) \tag{1.11}$$

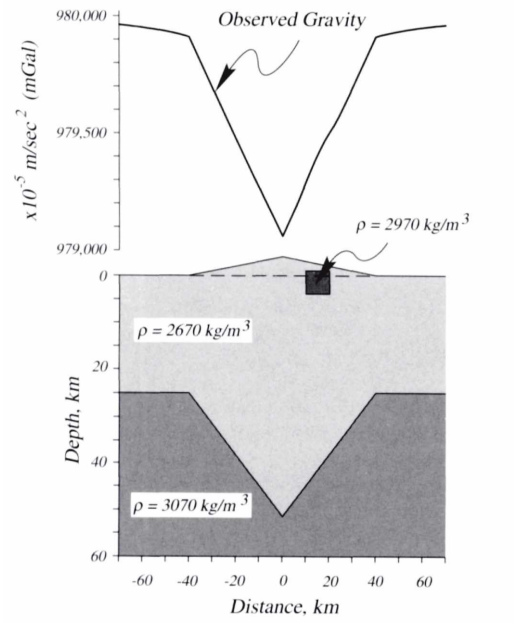

(a) First step: measured gravity g_z^o

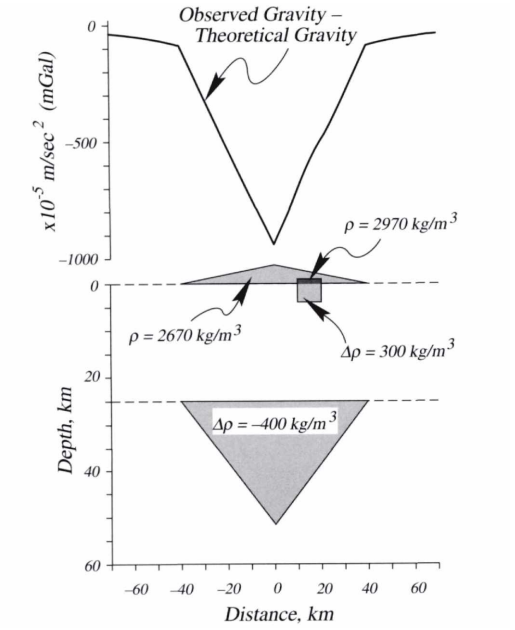

(b) Second step: remove the effect of the reference ellipsoid using equation 1.9

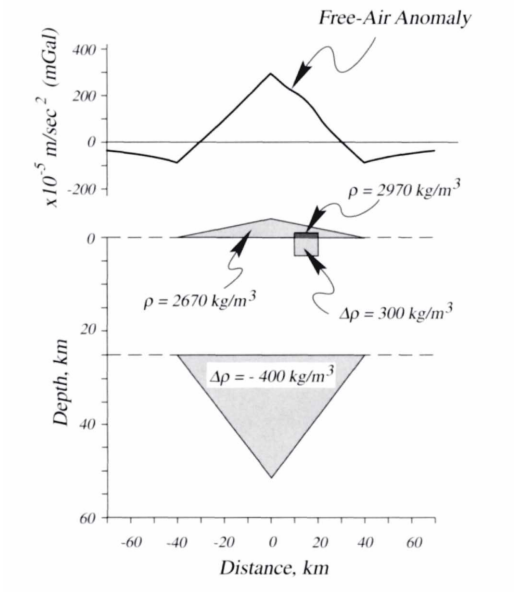

(c) Third step: apply the so-called free air correction

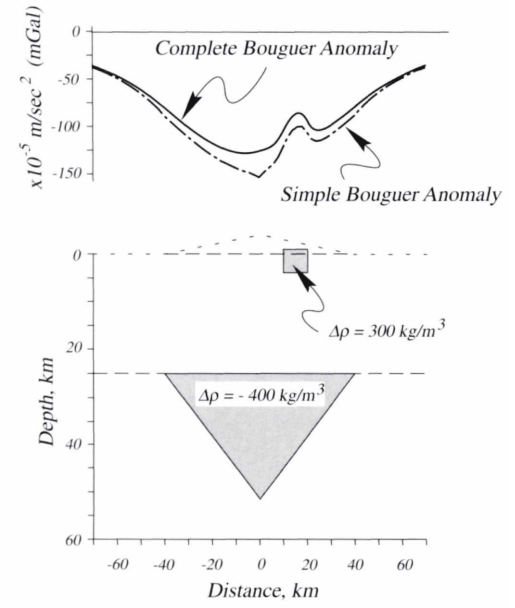

(d) Fourth step: apply the terrain correction to obtain the Bouger gravity-anomaly Δg_B^o

Figure 1.5: Example of gravity data preprocessing (Blackely, 1996)

1.3 Measurement principles and instruments

Since gravity is an acceleration, its measurement should simply involve determinations of length and time. However, such apparently simple task is not easily achievable at the precision and accuracy required in gravity surveying. Gravity in-

fluences a lot of physical phenomena. The instruments to measure gravity, called gravimeters or gravity meters, trade on one of those phenomena. In practical application the most widely method used are (Fedi and Rapolla, 1993):

1. static method, built with dynamometer principle (Hook's law):

$$m\mathbf{g} = k\mathbf{z} \tag{1.12}$$

where m is the proof mass, k is the spring elastic constant and $\mathbf{z}$ is the spring extension;

2. dynamic method, that rely on the measures of pendulum oscillations:

$$T = 2\pi\sqrt{\frac{L}{\mathbf{g}}} \tag{1.13}$$

where T is the oscillation period and L is the pendulum length. Another dynamic methods are those based on the law of falling bodies:

$$s = \frac{1}{2}\mathbf{g}t^2 \tag{1.14}$$

where s is the length of the path and t is the time elapsed.

Basically there are two kind of gravity measurement: absolute or relative. The former observes the absolute value of the gravity in a chosen place, as its name suggests. It requires long period observation, and usually absolute gravimeters are bulky and very expensive. The second method considers only differences in gravity acceleration between two or more points on the Earth surface. This technique is faster and the instruments are lighter and cheaper than absolute gravimeter. Moreover, in gravity anomaly interpretation there is no need to know the absolute value of gravity. Anyway thanks to network of gravity stations extended all over the word it's possible to estimate the absolute gravity trough relative measurement. The most import station's network is called *International Gravity Standardisation Net* (IGSN 71) and provides for each of the station the value of the absolute value.

1.3.1 Gravimeters

In order to reach the accuracy of μGal relative gravimeters are built with a proof mass suspended with an elastic system (e.g. a spring). The variation of the gravity generate a motion of the elastic system, thus measuring the change in position of the elastic system the acceleration variation is retrieved. In order to observe the vertical component of the gravity field the proof mass motion has only a degree of freedom. As consequence it can do a translation or a rotation. Based on the kind of movement allowed, the instrument are classified in static or stable in the first case, while unstable or astatic in the second one.

Stable or static gravimeters are basically spring balances carrying a constant mass. Variations in the weight of the proof mass linked to the variations in gravity cause the length of the spring to vary. The extension of the spring is proportional to the applied force, thus the gravity variation can be retrieved. In figure 1.6(a)

a spring of initial length s has been stretched by an amount δs as a result of an increase in gravity δg increasing the weight of the suspended mass m. The extension of the spring is proportional to the extending force, and recalling equation 1.12:

$$\begin{aligned} m\ \delta g &= k\ \delta s \\ \delta s &= \frac{m}{k}\delta g \end{aligned} \tag{1.15}$$

The elongation must be measured to a precision of $10^{-8}m$ in instruments suitable for gravity surveying on land. Although a large mass and a weak spring would increase the ratio m/k and, hence, the sensitivity of the instrument, in practice this would make the system liable to collapse. Consequently, some form of optical, mechanical or electronic amplification of the extension is required in practice. The necessity for the spring to serve a dual function, namely to support the mass and to act as the measuring device, severely restricted the sensitivity of this kind of gravimeters.

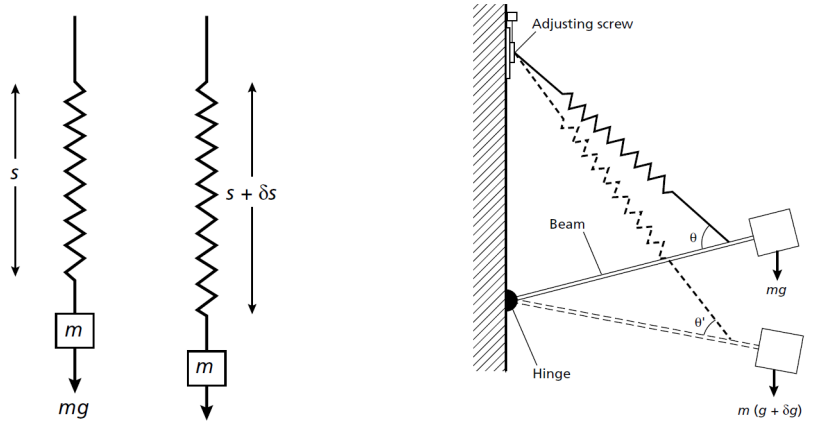

(a) Static gravimeter principle (b) Astatic gravimeter principle

Figure 1.6: Principle of measurements of the various kind of gravimeters used (Kearey et al., 2009)

The problem is overcome in modern unstable or astatic instruments which employ an additional force that acts in the same sense as the extension (or contraction) of the spring and consequently amplifies the movement directly. An example of an unstable instrument is the LaCoste and Romberg gravimeter (see figure 1.7). The meter consists of a hinged beam, carrying a mass, supported by a spring attached immediately above the hinge, as depicted in figure 1.6(b). The magnitude of the moment exerted by the spring on the beam is dependent upon the extension of the spring and the sine of the angle θ. If gravity increases, the beam is depressed and the spring further extended. Although the restoring force of the spring is increased, the angle θ is decreased to θ'. By suitable design of the spring and beam geometry the magnitude of the increase of restoring moment with increasing gravity can be made as small as desired. With ordinary springs the working range of such an instrument would be very small. However, by making use of a "zero-length" spring which is pretensioned during manufacture so that the restoring force is proportional to the physical length of the spring rather than its extension, instruments can be

fashioned with a very sensitive response over a wide range. The instrument is read by restoring the beam to the horizontal by altering the vertical location of the spring attachment with a micrometer screw. Thermal effects are removed by a battery-powered thermostatting system. The range of the instrument is 5000 $mGal$.

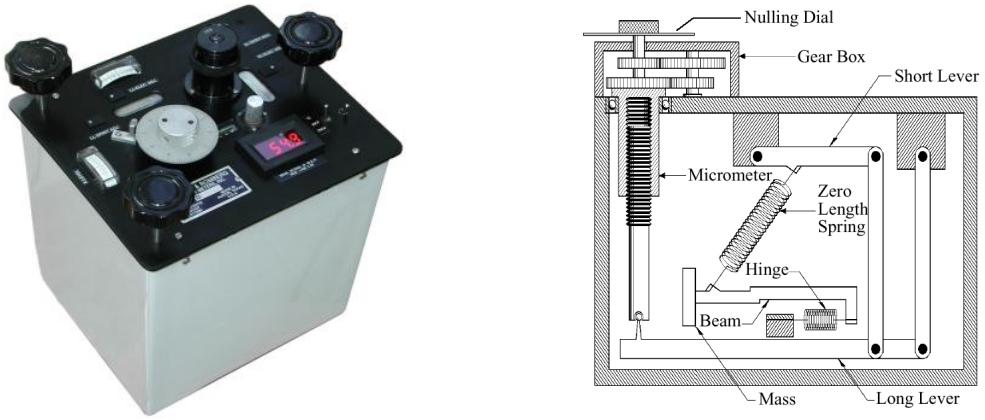

Figure 1.7: Lacoste-Romberg gravimeter,also available with μGal precision

The other unstable instrument in common use is the Worden-type gravimeter. The necessary instability is provided by a similar mechanical arrangement, but in this case the beam is supported by two springs.The first of these springs acts as the measuring device, while the second alters the level of the 2000 $mGal$ reading range of the instrument. In certain specialized forms of this instrument the second spring is also calibrated, so that the overall reading range is similar to that of the LaCoste and Romberg gravimeter. Thermal effects are normally minimized by the use of quartz components and a bimetallic beam which compensates automatically for temperature changes. Consequently, no thermostatting is required and it is simply necessary to house the instrument in an evacuated flask. The restricted range of normal forms of the instrument, however, makes it unsuitable for intercontinental gravity ties or surveys in areas where gravity variation is extreme.

1.3.2 Field techniques

During the field surveys the gravimeters are subjected to instrumental drift, due to thermal variation or to instrumental or spring hysteresis. The total effect can be of few $mGal$ per hour. The detection and correction of instrumental drift is based on repeated readings at a base station at recorded times throughout the day. The meter reading is plotted against time (figure 1.8) and drift is assumed to be linear between consecutive base readings. For each field measurement at a given time the drift correction value is subtracted from the observed value. To obtain a good correction interval of repetition of the observations on the base station must be between 1 and 2 hours. Measured drift can contain also moon and sun tidal effect. This effect can be removed in the same way of instrumental drift, otherwise a separately correction based on tables or software algorithms can be applied. The other big issue in the survey technique is the spacing of gravity stations that is critical to the subsequent

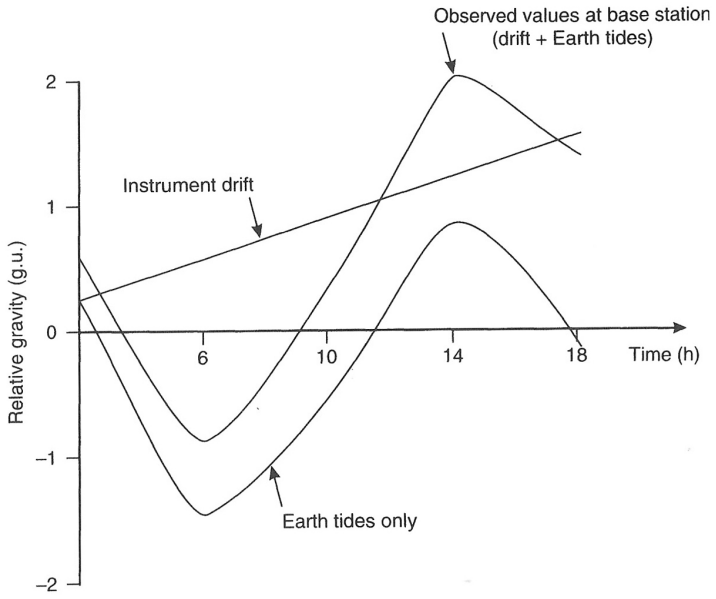

Figure 1.8: Graph of the effects of Earth tides and instrumental drift on the acceleration due to gravity (Reynolds, 1997)

interpretation of the data and depend on the final application of the survey. In fact in regional surveys only 2-3 station per km^2 are enough. The density of stations increases by reducing the dimensions of the investigated area. Typical value of spacing are 8-10 stations per km^2 in hydrocarbon exploration, 5-50 m when high resolution of shallow features is required, and less than 0.5 m in microgravimetry applications. To achieve the required accuracy (usually up to ± 0.1 $mGal$) a good quality in the point position is required. The most important coordinate is the elevation, where typically ± 10 mm is required. Historically this is a problematic task, because it implies long levelling network. Nowadays the problem is solved thanks to the diffusion and the precision improvement of GNSS. Differential positioning can achieve more than 1 cm accuracy in position determination (Leick, 1995). Other important challenges reached after the introduction of GNSS instrumentation are the airborne, better described in next paragraph, and the satellite gravimetry e.g. GOCE, CHAMP, GRACE). This technique allows costs reduction and increasing resolution in gravity surveying.

1.3.3 Airborne gravimetry

In the current paragraph the topic of airborne gravimetry is treated. It is of particular interest, because of its good benefits-costs ratio, velocity in surveying execution, final observation spatially defined on a regular grid. This last point is very useful for the inversion method treated in this thesis work, that is mainly developed to be used with airborne surveyed gravity data. Now on a brief history and basics principle are shown. For more details see e.g. Schwarz and Li (1997).

Airborne gravimetry is not a new topic in geodesy. Proposals to implement such a technique go back to the late fifties, for instance Thompson (1959), and first flight

experiments were done in the early sixties, Thompson and LaCoste (1960), Nettleton et al. (1960). The major obstacle to a successful implementation of such systems at that time was the inaccuracy of the navigational data, especially velocity and acceleration, which are needed to obtain the desired precision.

Although there were severe doubts at that time of ever achieving useful results with this method, see Hammer (1983), efforts to implement airborne gravimetry have continued, because airborne gravimetry at the appropriate level of accuracy is vastly superior in economy and efficiency to point-wise terrestrial methods. Geomagnetics is often quoted as an example. It was a marginal technique in geophysical exploration as long as it was ground-based. It developed into a major tool when is became airborne. As in gravimetry, it is not only the increased efficiency that brought this change about, but also the capability to survey remote areas, not easily accessible by land. In addition, airborne gravimetry is a technique which lends itself to spectral analysis because it is essentially based on the difference of two time series of measurements. By defining the spectral band of interest in advance, it is possible to develop operational procedures which will optimally resolve this band. This is important because the spectral band required in geodesy and geotectonics on the one hand, and in geophysical exploration on the other, is quite different, see Schwarz et al. (1992). By tuning operational procedures to the spectral band of interest, the estimated gravity profile will be of uniform accuracy and therefore well suited to be combined with gravity information from dedicated gravity satellite missions. They resolve the long wavelength features of the gravity field much better than terrestrial methods. This is especially important for many of the geodetic applications. When using terrestrial point gravity measurements, the resulting gravity field approximation will be non-uniform in accuracy, i.e. it will be extremely accurate at the measurement points and show interpolation errors which are a hundred times larger between the data points. To replace such a technique by one that has uniform accuracy over the whole range of interest, has numerous advantages.

Renewed interest in airborne gravimetry in the mid-eighties, led to improvements in scalar gravity system design, use of radar altimeters for vertical acceleration determination, and the selection of stable carriers to optimize operational conditions, see for instance LaCoste et al. (1982), Hammer (1983), Brozena (1984), LaCoste (1988). The system concept used in this development stage was that of a precise accelerometer stabilized in vertical direction by a damped platform system. This concept will be called scalar gravimetry in the following because only the magnitude of the gravity disturbance vector is determined in this case. Systems of this type produced the first useful results, although the accuracy of the navigational data remained a concern.

In the late eighties and early nineties advances in GPS technology opened new ways to resolve the navigational problems, see for instance Schwarz et al. (1989), Brozena et al. (1989), Kleusberg et al. (1990), Wei et al. (1992). The impact of this new technology led to two important developments. The first one was the perfection of existing scalar gravimeters to operational airborne gravity systems which could be used, on the one hand, for exploratory geophysical prospecting and, on the other hand, for large regional gravity surveys as required by geodesy and geotectonics. The second one was the development of new system concepts which made use of the

full potential of existing inertial measuring units (IMU) for sensor stabilization and gravity vector determination.

The use of INS in airborne gravimetry and the development of new system concepts was pioneered at the University of Calgary and at the Inertial Technology Centre (ITC) in Moscow. The concept of a gravity vector system was developed at the University of Calgary, see Knickmeyer (1990) and Schwarz et al. (1992), and was implemented as a stable platform system in cooperation with Sander Geophysics Ltd. At the same time, the ITC equipped an existing Russian platform with a highly sensitive vertical accelerometer and tested it for both scalar and vector gravimetry. Airborne tests with this system were done in Canada in cooperation between the ITC, the University of Calgary, and Canagrav Research Ltd. Results have been reported in Salychev et al. (1994) and Salychev (1995). The use of a strapdown INS for vector gravimetry was jointly explored by the University of Calgary and Canagrav Research Ltd. Its actual implementation was done by the University of Calgary and first results have been reported in Wei and Schwarz and Li (1996). Finally, the idea of a rotation invariant scalar gravimeter (RISC) which computes the magnitude of the gravity disturbance vector as the norm of its three vector components was developed in the early nineties and first published by Czompo in 1994. Results can be found in Czompo (1994) and Wei and Schwarz (1998). As is apparent from this brief overview, airborne gravimetry is a rapidly developing field and much of the development is rather recent. Although scalar gravimetry can be considered as a production technique, efforts are being made to improve its accuracy and wavelength resolution from current RMS values of $2-6\ mGal$ and half wavelengths of $5-10\ km$, to values of $1-2\ mGal$ and $3-4\ km$. Once these accuracies can be reliably achieved for large regional surveys, many tasks in geodesy and geotectonics can be solved efficiently and with homogeneous accuracy. Conceptually, gravity sensors used on the surface of the Earth or in its vicinity are highly sensitive accelerometers. In principle, as shown in paragraph 1.3.1, an accelerometer consists of a proof mass, a weightless elastic suspension, a case and a scale attached to the housing, see figure 1.9 for a simplified diagram of a possible realization. The proof mass m, considered as a point mass, is held in elastic suspension within the case. Assume that this can be done with three degrees of freedom, so that motion of the proof mass can be modelled in three-dimensional space. In an inertial frame of reference, the equation of motion for m can then be written as

$$m\frac{d^2\mathbf{r}_i}{dt^2} = m\ddot{\mathbf{r}}_i = \mathbf{F}_i + m\ \mathbf{G}\left(\mathbf{r}_i\right) \tag{1.16}$$

where r is the position vector from the origin of the inertial reference frame (i) to the centre of the proof mass m; $\mathbf{r}$ is thus the acceleration of the proof mass with respect to an inertial frame of reference and is often called absolute acceleration; $\mathbf{F}$ is the force causing the elastic deformation of the suspension; $\mathbf{G}\left(\mathbf{r}\right)$ is the sum of the Newtonian attraction on m due to all bodies in the universe. Note that the assumption of an inertial reference frame considerably simplifies the formulas because inertial forces, due to frame rotation, are not considered. For an observer in the measurement frame of the accelerometer case, only the elastic deformation force is observable and can be measured on the internal scale. By dividing equation 1.16

by m, one obtains

$$\ddot{r}_i = \frac{\mathbf{F}_i}{m} + \mathbf{G}(\mathbf{r}_i) \tag{1.17}$$

Setting

$$\mathbf{f}_i = \frac{\mathbf{F}_i}{m} \tag{1.18}$$

and rearranging this formula with respect to $\mathbf{f}$, results

$$\mathbf{f}_i = \ddot{\mathbf{r}} - \mathbf{G}(\mathbf{r}_i) \tag{1.19}$$

where $\mathbf{f}$, often called specific force, is the output of the spatial accelerometer. It has the unit of an acceleration because $\mathbf{f}$ is expressed as force per unit mass. The term on the left-hand side can be interpreted as representing the contact force exerted on the accelerometer by its support structure. The term on the right-hand side shows that $\mathbf{f}$ is the difference between absolute acceleration (i-frame) and net gravitational acceleration at m. Thus, a separation of $\mathbf{r}$ and $\mathbf{G}(\mathbf{r})$ appears not to be possible on the basis of measurements $\mathbf{f}$. However, experience shows that an accelerometer can be used as a relative gravimeter on the surface of the Earth. When it is set up at a point and aligned by levelling to the gravity vector at the point of support, the change of gravity relative to another point can be measured. This apparent discrepancy can be explained can be given in terms of Newton's third law. By putting the support structure of the sensor on the surface of the Earth, gravity becomes a reaction force, counteracting the pull of the gravity field on the case.

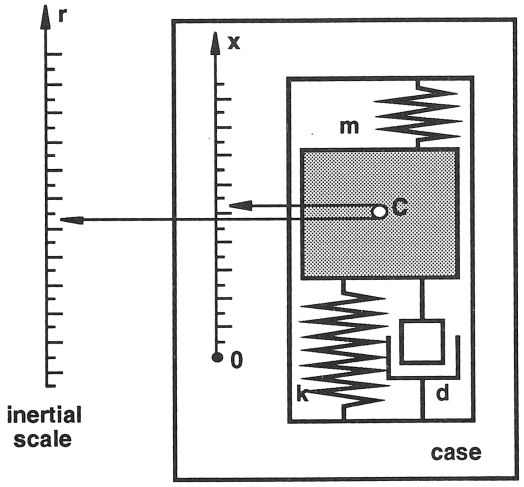

Figure 1.9: Principle of a linear mass-spring system (Schwarz and Li, 1997)

Thus, gravitational attraction and centrifugal force work as reaction forces and, thus, gravity is measured. Note, that this requires $\mathbf{r}$ to be known which is the case for a gravimeter stationary on the surface of the Earth if the rotation rate with respect to the i-frame is known. In a similar way, when such sensors are mounted in an aircraft the force needed to counteract the pull of the gravity field on the aircaft and thus on the support structure of the accelerometer is measured, together with aircraft motion and other inertial forces. For the following conceptual discussion,

the important point is that accelerometers, mounted in an aircraft are sensitive to gravity in the specific sense discussed above. It should also be noted that for any type of free-fall motion, the output of an accelerometer will always be zero, even if it occurs in a gravity field, see Jekeli (1992). In general, accelerometers are sensors which are only sensitive along one axis. One simple realization, the linear mass-spring system will be briefly discussed as an example. Its principle is shown in figure 1.9. Typically, three such sensors would be mounted in an orthogonal triad to measure the specific force vector. Coupling this system with a GPS antennas, the vector $\ddot{r}$ can be derived and thus the gravity value deduced. An example is shown in the graphs of figure 1.10.

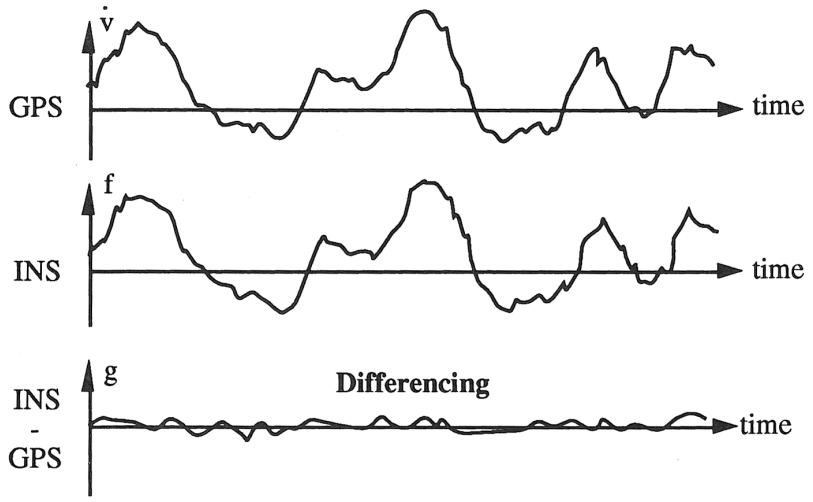

Figure 1.10: Principle of a linear mass-spring system (Schwarz and Li, 1997)

To give a conceptual framework to the following discussion, figure 1.11 will be used. It shows the different approaches to airborne gravimetry that have either been implemented or proposed. They fall into three major groups:

- Scalar gravimetry
- Vector gravimetry
- Gravity Gradiometry

In the rest of this paragraph, each of these implementations will be briefly described.

In scalar gravimetry the magnitude of the anomalous gravity vector is determined. The basic idea can be implemented in either one of three ways. First, a precise vertical accelerometer can be mounted on a stabilized platform. Changes in the accelerometer readings, corrected for vertical aircraft acceleration, are then the desired gravity changes. The orientation problem is solved by platform stabilization, the separation problem by differencing two acceleration measurements, of which one is sensitive to gravity and the other is not. Second, a strapdown system can be used where the equivalent of a platform stabilization is done by computing the rotation matrix between the body frame of the vertical, accelerometer and the local-level frame. In this case no separate accelerometer is used as gravity sensor, but the vertical accelerometer of the system is employed for this purpose. Again,

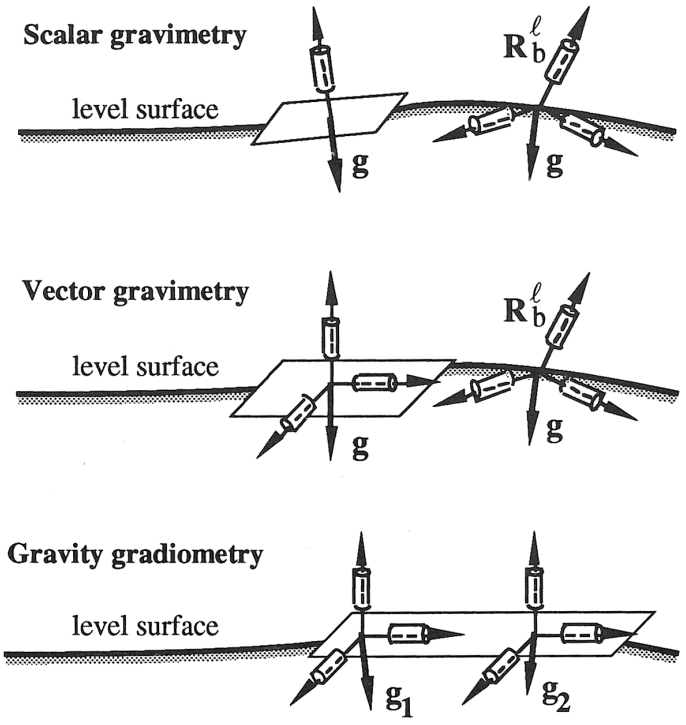

Figure 1.11: Approaches to airborne graviemty (Schwarz and Li, 1997)

its output has to be corrected for vertical aircraft acceleration. Finally, a triad of three orthogonal accelerometers can be used to obtain changes in the magnitude of gravity from changes in the difference between the specific force vector and the aircraft acceleration vector. In this case, the orientation problem is eliminated in theory and all three acceleration sensors contribute directly to the determination of gravity. The main difference between the three methods is the way in which the orientation of the accelerometers with respect to the local vertical is established. In principle, alternatives such as a GPS multi-antenna system or a star tracker, could also be applied. Furthermore, the absolute orientation problem can be replaced by a relative orientation problem. Instead of knowing the vertical orientation of one accelerometer in space, one has to know the relative orientation of two acceleration frames, namely that of the IMU local-level frame and the GPS local-level frame. Because no absolute orientation is needed in this case, the system has been called "Rotation Invariant Scalar Gravimeter (RISG)".

In vector gravimetry, the magnitude and direction of the anomalous gravity vector is determined. This can either be done by using a stable platform or a strapdown inertial system. In the first case, the accelerometers are essentially isolated from rotational motion and high resolution acceleration sensors with a relatively small measuring range can be used. Platform drifts are, however, a real problem because they affect the horizontal components directly and thus and quasi-systematic errors to the deflections of the vertical. Because the system works as a feedback mechanism, it is difficult to isolate these errors in post mission. In the second case, the accelerometer triad experiences full rotational motion and the error model becomes therefore much more complex. This is partially compensated for by the fact that

a high-rate digital output is available and that it is therefore possible to carefully analyze data post mission. The orientation and separation problems are solved in essentially the same way as in scalar gravimetry.

In airborne gravity gradiometry, the second-order gradients of the anomalous gravity potential are determined along the flight trajectory. By integrating them using GPS velocity, first-order gradients and thus the anomalous gravity vector can be obtained. Conceptually, these systems can be viewed as an assembly of two carefully aligned accelerometer triads on a common stable platform. Thus, the orientation problem is again solved by platform stabilization, while the separation problem is solved by differencing sensor outputs on a common base. Although gravity gradiometers require a much higher relative sensor accuracy than the systems discussed above, they are currently the only systems that offer the promise of resolving the high-frequency gravity spectrum with high accuracy because they do not require independent kinematic acceleration measurements.

In addition to the fundamental design problems of airborne gravimetry, major design changes are necessary when going from a stationary mode of operation to a dynamic one. The high accuracy of stationary gravimeters is due to the stable environment and the small measurement range. The first allows the averaging of measurements over time and thus results in improved accuracy. The second gives improved resolution. Airborne gravity meters have not only to function in high vibrational noise, which typically is a thousand times larger than the signal to be measured, but are also designed for operation under accelerations of 50 to 100 ms^{-2}. This severely limits the use of averaging techniques. Thus, resolution suffers and accuracy is affected. Measurement accuracies of better than 0.01 $mGal$, which are typically achieved with stationary field instruments, cannot be expected from systems working under these dynamic conditions. The current resolution to reliably achieve measurement accuracies of 1.5 $mGal$ at 5 km resolution is nowadays available.

Chapter 2

Gravity interpretation

The aim of the interpretation of gravimetric data is to determine the true model of the subsurface geology trough the determination of mass density distribution of anomalies and their geometrical shape. This is the most difficult step along the whole interpretation process. In fact, as already explained in chapter 1, the gravity signal has the property to relate the observation carried out in each point with the mass distribution and geometry of the whole investigate body, thus each observation depend from all the problem unknowns. In other word a change in a single parameter of the subsurface model influences the entire set of observation.

In some ideal cases there is an exact theory (Herglotz, 1907) that explain how the data should be treated in order to replicate the correct model. This schemes are valid only for few examples of limited applicability, because they are developed in ideal cases. Moreover, this technique may be often very unstable. The last issue is that in many inverse problems the model that one aims to determine is a continuous function of the space variables. This means that the model has infinite degrees of freedom but, in a realistic experiment, the amount of data that can be used is obviously finite: a simple count of variables shows that data cannot carry sufficient information to determine the model uniquely and so there are many models that explain the data equally well. A classical example is the interpretation of gravity field measurements around a planet; in fact given the distribution of masses inside the planet, it is simple to predict uniquely the values of the gravity field around the planet (forward problem), but there are different distributions of masses inside the planet that give exactly the same gravity field in the space. The stability and the uniqueness are the most tricky problem to be faced in the inverse solution.

In the current chapter the gravity interpretation techniques, classified as direct or indirect, will be discussed. The division is based on how observed data play their role in the recovering process: direct methods use the data to estimate the model parameters trough the inversion of observation equations. That's why they are often called inverse methods. On the contrary, indirect solutions don't rely on the observation, which aren't used in the parameters determination. The common approach used is a trial and error one, where forward model with parameters determined on geological information and site conformation is recurrently computed and compared with the set of observations.

2.1 Forward model

The forward model is the mathematical relationship between the observable quantities and the model parameters. In case of gravimetric interpretation observable are the gravity anomalies, while the parameters to be estimated are the mass density distribution and the geometry of the investigated body. The fundamental equation of the model is derived from 1.3. In particular, the most used is the radial or plumb line component of the field g_Z. It can be computed trough the gravitational potential and its expression in a local cartesian coordinates system (Blackely, 1996) for a generic point P of coordinates x, y, z is given in equation 2.1.

$$g_Z(P) = \frac{\partial V(P)}{\partial z} = -G \int_{x'} \int_{y'} \int_{z'} \rho(x', y', z') \frac{(z - z')}{(r)^3} dx' dy' dz' \tag{2.1}$$

where $r = \sqrt{(x - x')^2 + (y - y')^2 + (z - z')^2}$
Equation 2.1 can be reformulated with the following general expression:

$$g_Z(P) = \int_{x'} \int_{y'} \int_{z'} \rho(x', y', z') \psi(x - x', y - y', z - z') dx' dy' dz' \tag{2.2}$$

The integral expressed in equation 2.2 is a convolution integral, but its computation is not a simple task for real complex geological bodies. In fact, an analytical solution exists only for very simple geometric shapes like point masses, spheres, slabs, prisms, etc. Hence, if the investigated body cannot be described by one of those simple models usually its volume is divided into compartment built with a series of this simple geometries. Now, the total signal of a body can be derived with the recurs to

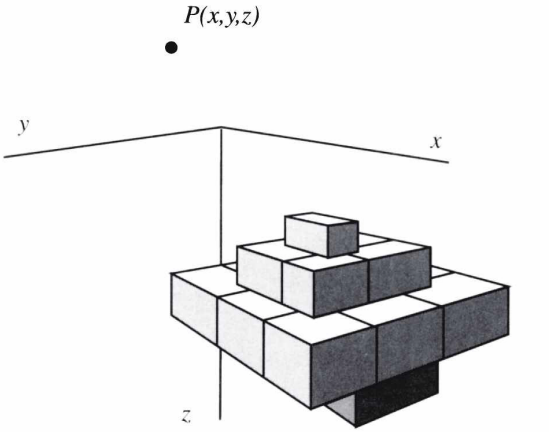

Figure 2.1: Example of subdivision of a body in compartments using regular prisms. The point $P(x, y, z)$ is the computational point (Blackely, 1996)

the effects superposition principle and the integral expressed in equation 2.2 become a simple summation of the signal generated by each one of the single i^{th} constant density compartments composing the body. The general expression of the whole signal assume the form showed in equation 2.3.

$$g_Z(P) = \sum_{i=1}^{N} \rho_i \psi_{Pi} \tag{2.3}$$

The function ψ_{Pi} describes the geometry of the model and depends from the basic chosen shape to built the whole geology. The density ρ_i is considered constant in every compartment. It is equivalent to samples the density distribution function with a step with the dimension of a single simple component. Clearly, the resolution of the density function is strongly related to the approximation chosen. It's evident that in the final formulation there is a linearly dependency of the gravity signal from the density contrast of the subsurface, but non linear respect the geometry, that is function of the operator ψ.

Next sections describes the vertical component of the gravity signal generated by a series of simple three-dimensional geometric shapes. They are the most widely used in subsurface modelling: the point mass, the rectangular prism, and the tesseroid. Those approximation are good both for very localized and small investigation areas and for regional extension gravity field description.

2.1.1 Point mass

The point mass approximation is the simplest way to describe a compartment of the modelled geological structure. In fact it places the whole mass of the cell in a point, usually its barycentre. The expression of the generated signal is very simple and is derived directly from Newton's law of universal gravitation, stated in equation 1.2: the acceleration is projected on the requested direction, in the most of gravity surveying case this is direction of the plumb line. In a generic point P the signal generated from a generic mass m positioned in the origin of a cartesian reference system can be expressed as:

$$g_Z(P) = Gm\frac{\mathbf{r_P}}{|\mathbf{r_P}|^3} \cdot \mathbf{k} = Gm\frac{1}{r_P^2}\cos\psi \tag{2.4}$$

where $\mathbf{k}$ is the versor pointing in the z axis direction and ψ is the angle between the position vector $\mathbf{r_P}$ of P and the z axis as presented in figure 2.2.

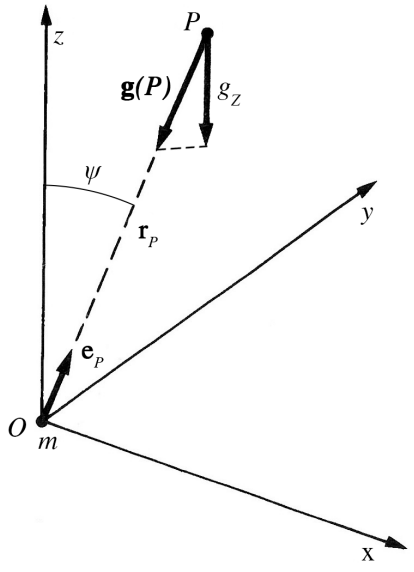

Figure 2.2: Geometry of a point mass positioned in the origin of a cartesian reference frame

2.1.2 Rectangular prism

The prisms is an important geometric shape because it can approximate any density distribution with the desired resolution. On the other hand it is reliable only in planar approximation, thus becoming applicable only for small areas (Nagy, 1966). In order to retrieve the gravitational signal of the prism it's useful to move

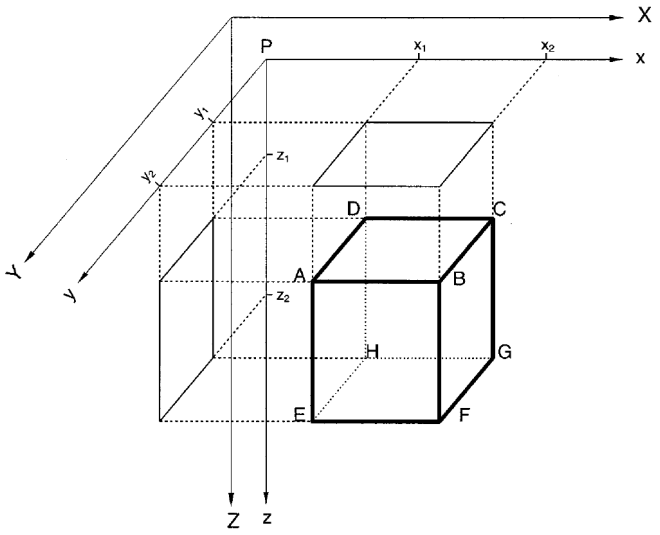

Figure 2.3: Prism geometry (Nagy et al., 2000)

the origin in the computation point P, thus the coordinates of the prism corner become as shown in figure 2.3:

$$\begin{aligned} x_1 &= X_1 - X_P \\ x_2 &= X_2 - X_P \\ y_1 &= Y_1 - Y_P \\ y_2 &= Y_2 - Y_P \\ z_1 &= Z_1 - Z_P \\ z_2 &= Z_2 - Z_P \end{aligned}$$

this simplification can be done without any loss of generality. The gravitational potential is generally expressed as:

$$U(P) = u(P)\ G\ \rho \tag{2.5}$$

where the therm $u(P)$ come from the volume integral depicted in equation 2.6.

$$u(P) = \int_{x_1}^{x_2} \int_{y_1}^{y_2} \int_{z_1}^{z_2} \frac{dxdydz}{r} \tag{2.6}$$

The solution of this triple integral over the prism volume can be given in the form of equation 2.7. The result is a continuous function in the whole $\mathbb{R}^3$ as its first order derivatives. The derivation of the formula is not subject of the current discussion.

The interested readers can find a detailed explanation in Bessel (1813) or Haáz (1953).

$$u(P) = \left|\left|\left| xy \ln(z+r) + yz \ln(x+r) + zx \ln(y+r) \right.\right.\right. \\ \left. - \frac{x^2}{2} \arctan \frac{yz}{xr} - \frac{y^2}{2} \arctan \frac{zx}{yr} - \frac{z^2}{2} \arctan \frac{xy}{zr} \right|_{x_1}^{x_2} \Bigg|_{y_1}^{y_2} \Bigg|_{z_1}^{z_2} \quad (2.7)$$

The vertical component of the gravity field of the rectangular prism can be obtained differentiating the potential u expressed in equation 2.7 respect the z coordinate, thus obtaining:

$$g_Z(P) = \frac{\partial u(P)}{\partial z} = \left|\left|\left| x \ln(y+r) + y \ln(x+r) - z \arctan \frac{xy}{zr} \right|_{x_1}^{x_2} \Bigg|_{y_1}^{y_2} \Bigg|_{z_1}^{z_2} \right. \quad (2.8)$$

The same result can be derived starting from vertical gravity component formulation depicted in equation 2.2 considering ρ constant in the prism.

Due to its numerical form, equation 2.8 cannot be calculated all over the space. The corners of the prisms suffers of this indeterminacy, but zero limits for the critical terms in the equation exist at this place. Consequently g_Z can be extended in $\mathbb{R}^3$ continuously. If P is located in a corner of the prism, for example point D in figure 2.3, where g_Z is not defined equation 2.8 become:

$$g_Z(P) = \lim_{(\varepsilon_1,\varepsilon_2,\varepsilon_3)\to(0,0,0)} \left|\left|\left| x \ln(y+r) + y \ln(x+r) - z \arctan \frac{xy}{zr} \right|_{\varepsilon_1}^{x_2+\varepsilon_1} \Bigg|_{\varepsilon_2}^{y_2+\varepsilon_2} \Bigg|_{\varepsilon_3}^{z_2+\varepsilon_3} \right. = \\ = x_2 \ln(y_2 + r(x_2, y_2, z_2)) - x_2 \ln(y_2 + r(x_2, y_2, 0)) - x_2 \ln(r(x_2, 0, z_2)) + \\ + x_2 \ln(r(x_2, 0, 0)) + y_2 \ln(y_2 + r(x_2, y_2, z_2)) - y_2 \ln(y_2 + r(x_2, y_2, 0)) + \\ - y_2 \ln(y_2 + r(0, y_2, z_2)) + y_2 \ln(y_2 + r(0, y_2, 0)) - z_2 \arctan \frac{x_2 y_2}{z_2 r(x_2, y_2, z_2)} \quad (2.9)$$

To extend the usage of prisms also to large areas, the gravity attraction can be expressed in a geographic coordinates system, that is the vertical direction becomes the radial one. This can be done using the well known geodetic relationship existing between a local cartesian coordinates system and the geographical coordinates system.

2.1.3 Tesseroid

The tesseroid or spherical prism is an elementary body useful to describe the subsurface in ellipsoidal or spherical approximation. It become essential when the dimensions of the modelled area don't allow the planar approximation and so prism cannot be used. In practice it is a segment of a sphere delimited by two meridians with longitude λ_1 and λ_2, two parallels with latitude ϕ_1 and ϕ_2, and two spheres whit radius r_1 and r_2, or considering R the radius of the reference sphere or ellipsoid

$R+h_1$ and $R+h_2$. The figure 2.4 depict the boundary and the shape of the tesseroid just explained.

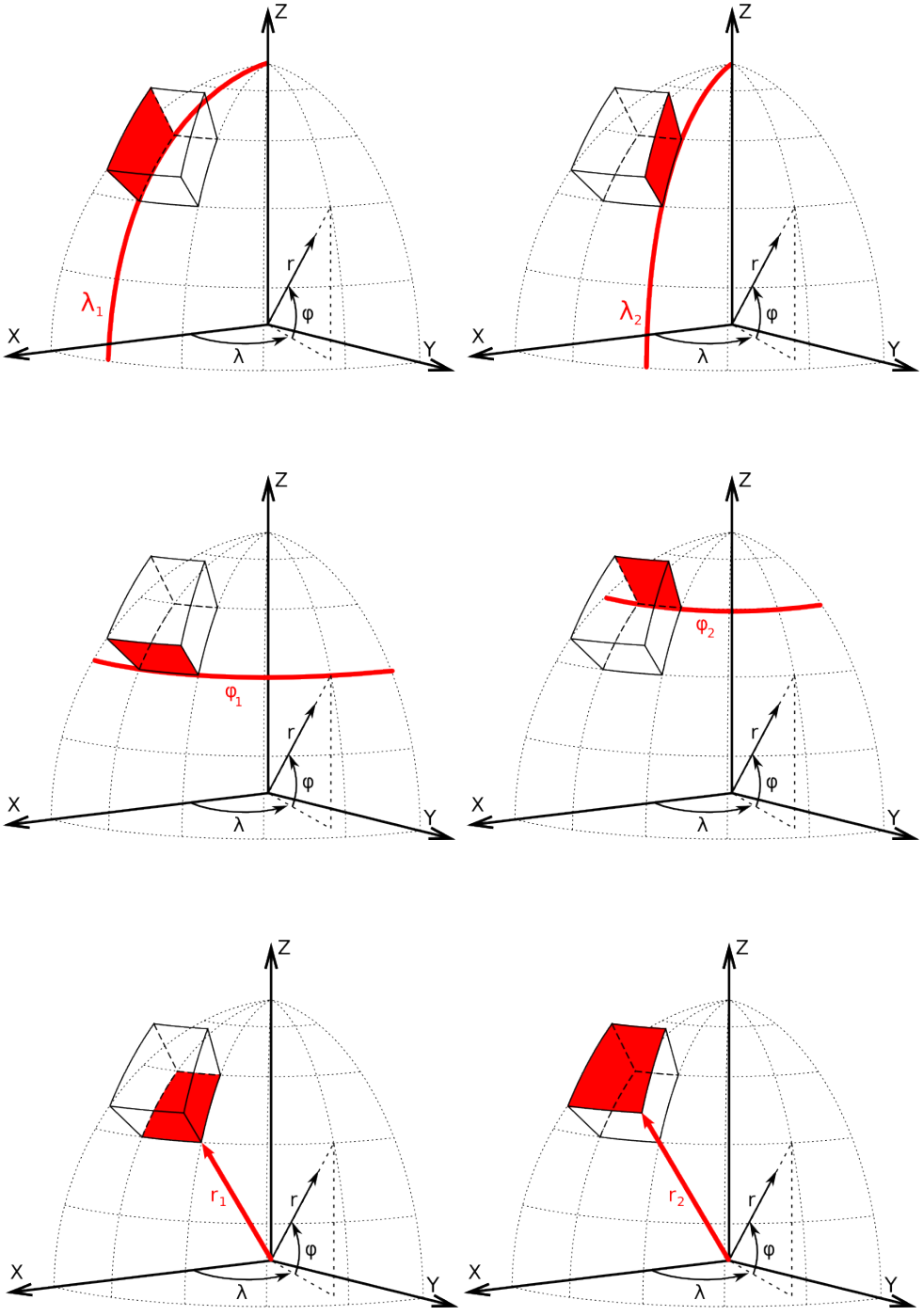

Figure 2.4: Tesseroid boundaries in spherical reference frame (Uieda, 2013)

The computation of the tesseroid gravitational potential and its gravitational attraction in usually performed in a global geocentric coordinate system (X, Y, Z) or local east, north, up coordinate system (x, y, z) in a generic point P of coordinates φ, λ, r, as shown in figure 2.5.

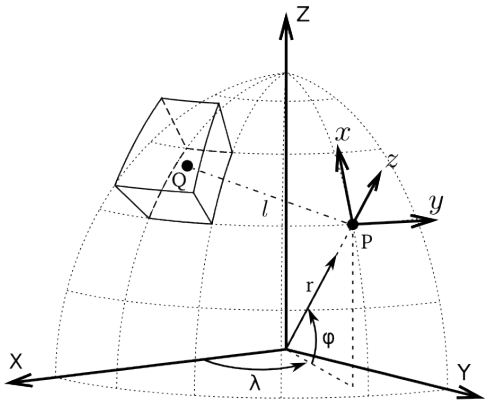

Figure 2.5: View of a tesseroid, the running integration point $Q(\varphi', \lambda', r')$, the computational point $P(\varphi, \lambda, r)$, and the global and local coordinates system. (Uieda, 2013)

The gravitational potential of the tesseroid can be calculated with equation 2.10, derived from the newtonian potential expressed in spherical coordinates for the volume of a generic tesseroid, that is delimited by φ_1, φ_2, λ_1, λ_2, r_1, and r_2 (Heck and Seitz, 2007; Grombein et al., 2013).

$$V(r, \phi, \lambda) = G\rho \int_{\lambda_1}^{\lambda_2} \int_{\phi_1}^{\phi_2} \int_{r_1}^{r_2} \frac{r'^2 \cos\varphi'}{\ell} \, dr' d\phi' d\lambda' \tag{2.10}$$

where $\ell = \sqrt{r'^2 + r^2 - 2r'r\cos\psi}$ denotes the Euclidean distance between the computation point $P(\varphi, \lambda, r)$ and the running integration point $P(\varphi', \lambda', r')$, and ψ is the angle between the position vector of P and Q, respectivelyr_P and r_Q, computed as $\cos\psi = \sin\varphi \sin\varphi' + \cos\varphi \cos\varphi' \cos(\lambda' - \lambda)$.

From the potential depicted in equation 2.10 the radial gravitational attraction, that is the vertical attraction in a local reference system, can be derived as follows:

$$g_z(r, \phi, \lambda) = -\frac{\partial V(r, \phi, \lambda)}{\partial r} = G\rho \int_{\lambda_1}^{\lambda_2} \int_{\phi_1}^{\phi_2} \int_{r_1}^{r_2} \frac{r - r'\cos\psi}{\ell^3} r'^2 \cos\varphi' \, dr' d\phi' d\lambda' \tag{2.11}$$

This integral cannot be solved analytically but need to be evaluated numerically. As an alternative, the gravitational effect of distant tesseroids can be calculated using a Taylor expansion of the integral kernel of the equation 2.11 at $P_0(\varphi_0, \lambda_0, r_0)$

$$L(r', \varphi', \lambda') = \frac{r'^2 (r - r'\cos\psi)\cos\varphi'}{\ell^3} = \\ = \sum_{i,j,k} L_{ijk} (r' - r_0)^i (\varphi' - \varphi_0)^j (\lambda' - \lambda_0)^k \tag{2.12}$$

where

$$L_{ijk} = \frac{1}{(i+j+k)!} \frac{\partial^{i+j+k} L(r', \varphi', \lambda')}{\partial r'^i \partial \varphi'^j \partial \lambda'^k} \Bigg|_{\substack{r'=r_0 \\ \varphi'=\varphi_0 \\ \lambda'=\lambda_0}}$$

The specific choice of the point P_0 allows only the terms with even power remain in the Taylor series expansion, thus combining the result obtained in equation 2.12 and

equation 2.11 the radial gravity attraction of the tesseroid can be finally expressed as:

$$g_z(r,\varphi,\lambda) = G\rho\Delta r\Delta\varphi\Delta\lambda\left[L_{000} + \frac{1}{24}\left(L_{200}\Delta r^2 + \right.\right. \\ \left.\left. + L_{020}\Delta\varphi^2 + L_{002}\Delta\lambda^2\right) + \mathcal{O}\left(\Delta^4\right)\right] \quad (2.13)$$

2.1.4 Remarks

The presented simple geometrical shapes can be used to compose complicated geological situation thus modelling the subsurface. The final quality depends mainly from the dimension of each elementary cell, that is the discretization step. But, also the geometric cell shape play its fundamental role. In fact each of the presented elementary body presents some limitation. The three main issue in the choice of the basic shape of the model are the required computational time, the achievable precision and the approximation errors.

In order to compare the different shape an equality criterion is needed. Hence, the dimensions of the "equivalent" prism are computed from the dimensions of the tesseroid and the basic assumptions are that the mass of the two different shapes are equal at the first-order and they have the same density. Ignoring the terms of order $\mathcal{O}\left(\Delta^2\right)$ the approximation error induced depends on the size of tesseroid (Heck and Seitz, 2007). The prisms formulas presented in paragraph 2.1.2 are analytical solutions, but in spherical reference frame the dimension of the prisms must be calculated directly from the tesseroid extension since usually the terrain data are given in geodetic coordinates. That's why usually the tessereoid is used.

Furthermore, tesseroid signal computation is faster than prisms up to ten time faster. This remarkable difference is caused by time consuming of the *log* and *arctan* function calls in the analytical solution of the prism. The point mass are faster, but less accurate in the signal reproduction, thus they may be used to compute the far zone contribution. Computational time for the three models are shown in in figure 2.6 where a test done by Heck and Seitz (2007) using the JGP95 global DTM (Lemoine et al.) is summarized.

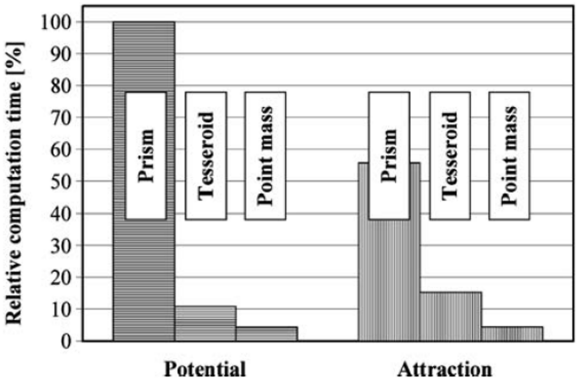

Figure 2.6: Comparison of the computational time using tesseroid, prism or point mass to compute potential and gravitational attraction (Heck and Seitz, 2007)

The outcome is that in ellipsoidal or spherical coordinates system tesseroid discretization of the subsurface is widely preferred due to its low time-consuming during computation and to its implicit description of the spherical geometric, at the price of approximation due to Taylor series expansion. On the other hand prisms, if used in spherical coordinates, suffers of approximation due to the shape, that more or less are comparable with those introduced with tesseroid. In planar approximation prisms are the better solution tanks to the existence of an analytical solution and the particular geometry that they represent very well; in fact in a local cartesian system there are no empty space between prisms, like if their are used in spherical or ellipsoidal reference frame.

Finally, point mass seems better respect all the other in term of computational time. This is true only if they are used with the same resolution of prisms or tesseroids, but to obtain a good results in terms of accuracy of the modelled signal at a nearest distance they need to be denser and positioned in "strategic" point. Time consuming increases and there are no other advantages in this choice, except if they are used for far masses signal.

A detailed comparison of the three method used to describe the subsurface and to model gravitational attraction and potential can be found in Heck and Seitz (2007).

There are also a series of methods called Fourier methods that are based on the Fourier transform. In fact Fourier transform is a very fast technique to compute convolution integrals. Fortunately, all the general formulations of quantity used in gravity prospecting, like the gravitational attraction expressed in 2.18, are of this kind. The disadvantage is that it requires only gridded data. For details see Heiskanen and Moritz (1967), Fedi and Rapolla (1993), Blackely (1996), Hofmann-Wellenhof and Moritz (2006), or Sansò and Sideris (2012).

2.2 Uniqueness and stability of solution in gravity interpretation

As already said in the introduction of this chapter there are two trivial issues that in general may affect all the inversion problems: the uniqueness and the stability of the solution. The aim of this section is to give a description on the effects of this issue in the solutions and the possible methods to reduce their influence.

The inversion problem can be formalized with a set of equation that link the observations to the set of parameters; consider a vector of observation $\mathbf{y} \in \mathcal{R}^m$, a vector of unknown parameters $\mathbf{x} \in \mathcal{R}^n$, the relation between $\mathbf{x}$ and $\mathbf{y}$ is given by:

$$\mathbf{y} = A(\mathbf{x}) \tag{2.14}$$

where $A(\mathbf{x}) : \mathcal{R}^m \mapsto \mathcal{R}^n$ is a known vector function (e.g. equation 2.21 with ψ given by equation 2.8). Now on, for sake of simplicity $A(\mathbf{x})$ will be consider a linear relationship. If it isn't there is always the possibility to linearize the system around an approximated value. As already seen, the estimation of $\mathbf{y}$ trough a known parameters set $\mathbf{x}$ is called forward problem. It usually admits always an unique solution and often the problem is well-posed, that is a little variation in $\mathbf{x}$ causes only a little variation in $\mathbf{y}$. The aim of an interpretation problem is the opposite:

estimate $\mathbf{x}$ using the observations vector $\mathbf{y}$, that usually is corrupted by additive noise $\boldsymbol{\upsilon}$. The general model stated in equation 2.14 become:

$$\mathbf{y} = A\mathbf{x} + \boldsymbol{\upsilon} \tag{2.15}$$

where, under the linear hypothesis, A is a matrix of dimensions $m \times n$. This kind of problem may be ill-posed, that is the solution suffers of instability or nonuquiness. It means the A is ill-conditioning matrix. The instability is a very tricky problem because of the big and unrealistic variations of the estimated solution $\mathbf{x}$ caused by little variations in the data $\mathbf{y}$. In the language of linear systems analysis, A is a linear functional of $\mathbf{x}$. If i and j are respectively row and column index of A for all $i \neq j$, A is a smoothly varying function. Hence, $\mathbf{y}$ is always "smoother" than $\mathbf{x}$ as long as the observation point is outside the source body. Consequently, the inverse problem of deriving $\mathbf{x}$ from equation 2.15 amounts to an "unsmoothing" of $\mathbf{y}$. That's why the solution become unstable. There are ways to reduce the instability, but only at the expense of giving up information about the source. Instead, the nonuniqueness is a well known problem in gravimetric inversion. From the one hand it is related to the fact that usually the parameters are function, namely they have infinite degree of freedom, but the set of observations is finite. On the other hand is an intrinsic nonuniqueness of problems like determine the density distribution from gravity observations. In fact it's well known that for a given potential it's possible to determine an infinite series of mass distribution, as Gauss theorem states (Fedi and Rapolla, 1993).

Hansen (1998) categorized the ill-posed into two classes, respect the nature of the ill-conditionig of A:

- the problem is rank-deficient if the matrix A has one or more very small singular values and there is a well-determined jump between large and small singular values. This indicates that there are columns (or rows) that are nearly linear combinations of remaining columns (or rows).
- in discrete problems the singular values of A decay gradually to almost zero without particular jumps in the singular value spectrum.

A measure of the degree of ill-conditioning of the matrix A is described by the condition number that is the ratio between the relative change in the norm of the solution vector $\mathbf{x}$ to the relative change in the norm of y:

$$\begin{aligned} \frac{\|\Delta\mathbf{y}\|}{\|\mathbf{y}\|} &= \operatorname{cond}(A)\,\frac{\|\Delta\mathbf{x}\|}{\|\mathbf{x}\|} \\ \operatorname{cond}(A) &= \|A^{-1}\| \cdot \|A\| \end{aligned} \tag{2.16}$$

If $\|\cdot\|$ is the Euclidean norm, the condition number is given by the ratio between the maximum and the minimum singular value of A respectively. In addition, according to Hadamard (1902) and Hadamard (1923) a problem is ill-posed if a unique solution does not exist for all $\mathbf{y}$ or if the solution does not depend continuously on the data. If the number of observations m is smaller than the number of parameters n and the row vectors of A are linearly independent, the condition number $\operatorname{cond}(A)$ is not necessarily large but the problem is ill-posed in the sense of Hadamard, namely the problem has infinitely many such solutions that are perfectly consistent with

the data. To solve inverse problem several approaches have been studied, in any case if the problem is ill-posed additional information about the solution must be incorporated in order to stabilize the problem. Classical methods to solve inverse problems are the least squares methods (LS). Consider the problem of finding an approximate solution $\hat{\mathbf{x}}$ for the set of equations 2.15 where the unknown error term contains measurement errors and truncation errors in finite precision systems. An exact solution may not exist if $\mathbf{y}$ is not in the image space of the map A. The least squares solution of the system of equations 2.15 is the minimizer of the norm of the residual, i.e:

$$\hat{\mathbf{x}} = \min_{\mathbf{x}} \|\mathbf{y} - A\mathbf{x}\|^2 \tag{2.17}$$

If $A(\mathbf{x})$ is non-linear with respect to the parameters $\mathbf{x}$, the solution is sought iteratively. If the problem is ill-posed (i.e. cond(A) is very large), an unique solution does not exist or the solution is unstable. The algorithms that are used to stabilize the problem are called regularization methods. Examples of regularization methods are the truncated single value decomposition (Hansen, 1987) and Tikhonov regularization proposed by Tikhonov (1963) for stabilizing ill-posed problems arising in solving Fredholm integral equations of the first kind. A similar approach was independently proposed by Phillips (1962) and it was later reformulated by Twomey (1963). In the standard form of Tikhonov regularization the objective is not to find the minimizer of the norm of the residual but accept small deviation from the minimum to find a solution with smaller norm.

In some applications it may be appropriate to set certain equality or inequality constraints for the solution. Constrained LS problems are discussed and algorithms are given e.g. in Kaipio and Somersalo (2005). Under some restrictive assumptions is possible to guarantee the uniqueness of the solution at the gravimetric inversion. In particular, in a two layers model as that depicted in figure 2.7, only three cases can be distinguished and what one can estimated uniquely is:

- the density of one of the two layers (e.g. $\rho_C(\xi)$ or), once geometry ($D(\xi)$), topography ($H(\xi)$), and density of the other one (e.g. $\rho_C(\xi)$) were fixed;
- geometry of the surface between the two layers, if density of the two and topography are known;
- vertical gradient of density, when geometry of the surface between the layers, topography and density of the upper level are given.

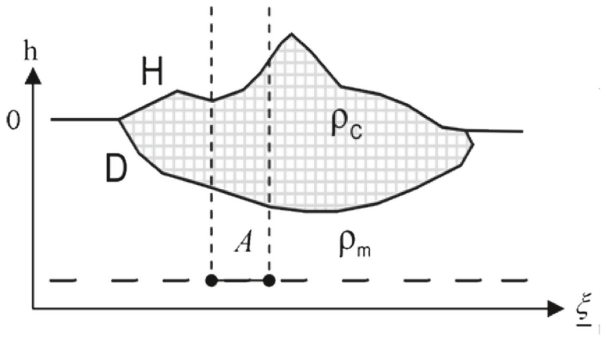

Figure 2.7: Two layers model of crust and mantle (Sampietro and Sansó, 2012)

Notice that those restrictive assumption doesn't remove the instability of solution, due mainly to the fact observation done on a plane are used to estimate three-dimensional parameters. As consequence a regularization method must be applied to the inversion system, but in this way there is the certainty that the true solution is well approximated. This uniqueness theorems are widely discussed in Sampietro and Sansó (2012), Biagi and Sansò (2003, 2004a,b), and Biagi (1997).

2.3 Indirect solutions

The main characteristic of indirect solutions is that the final value of the parameters is not deduced directly from data. In fact the observations are used only to test the goodness of the chosen solution, since indirect methods are essentially based on the trial and error approach.

A trial and error technique consists in the computation of the forward model, expressed in equation 2.2, of some geological situation a-priori chosen on the base of external knowledge on the area. Hence, the calculated theoretical signal is compared with the observed one in order to discover the shape and the density contrast of the geological anomalies that best describes the observations, on the base of a chosen best fit rule – e.g. minimum square distance. After that an operator adjusts by hand the parameters of the source, usually density distribution and geometry, in order to improve the quality of the solution (see figure 2.8).

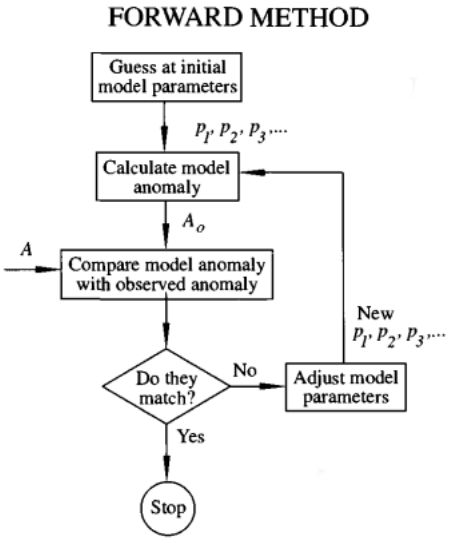

Figure 2.8: Forward techniques to interpret potential field data. Measured anomaly is represented by A, calculated anomaly by A_0, and transformed measured anomaly by A'. Parameters p_1,p_2,... are attributes of the source, such as depth, thickness or density (Blackely, 1996)

This kind of adjustment procedure is driven mainly by geological intuition and by the interpreter experience. As a consequence it cannot be automatized. Geological information is at the base of this process and is needed in order to discriminate between solutions that are possible, under the formal mathematical point of view, but improbable with respect to the field characteristics.

The pros of this classes of solution is the possibility to represent geological structure that are more complex than in the indirect methods. Obviously the most complex is the chosen forward model, the most optimization of calculation of the integral of equation 2.2 is needed in computer algorithms. As already said, it is common practice to divide the ore body in compartments, thus obtaining a discretized formulation of the integral that become more suitable for the PCs.

2.4 Direct solutions

Direct solutions use directly the observations during the estimation of the parameters of the model. Those methods insert the observation term – in this case g_Z^o – on the left of the forward equation and solves for some parameters of the model. That's why this class of solutions is also called inverse problem. The fundamental equation is the forward model (2.2), expressed in its general formulation as:

$$g_Z(P) = \int\int\int_{v_Q} \rho(Q)\,\psi(P,Q)\,dv_Q \tag{2.18}$$

that in a cartesian reference system, where point P has coordinates x, y, z and the running point Q x', y', z', become:

$$g_Z(P) = \int_{x'}\int_{y'}\int_{z'} \rho(x',y',z')\,\psi(x-x',y-y',z-z')\,dx'dy'dz' \tag{2.19}$$

The presented formulation of the forward model of gravity anomalies the term $\rho(x',y',z')$ accounts for the involved physical quantity – i.e. the mass density distribution – while $\psi(x-x',y-y',z-z')$ describes the geometry of the problem. Clearly, the aim of the inversion must be the mass or the geometry retrievement. Thus the solutions can be classified in *linear inverse problem* or *nonlinear inverse problem* on the base of the relationship between the observable and the parameters. Essentially, a linear inverse problem has the aim of mass estimation, while the nonlinear one is interested in geometry.

2.4.1 Linear inverse problem

Since the mass distribution is a linear function of the gravity signal its estimation is called linear inverse problem. The simplest approach to the problem is the estimation of a single average density with known geometry. In this case equation 1.1 for a generic point P become:

$$g_Z(P) = \bar{\rho}\psi(P) \tag{2.20}$$

With a series of N measures of gravity anomalies and a simple linear regression the average density $\bar{\rho}$ can be determined. A detailed discussion of this solution can be found in Ishihara (1989) or Plouff (1976).

As already seen in section 1.1, the situation can be complicated and the geological structure divided into small compartments or cells (see figure 2.9). Hence, equation

2.18 could be rewritten as the sum of a series of discrete terms.

$$g_{Z_i}(r_i) = \sum_{j=1}^{n} \rho_j \psi_{ij}(r_j, r_i) \tag{2.21}$$

Of course, geology is never so simple and the results almost certainly will be no accurate. Now, assembling all the m observations it's possible to write system:

$$\underset{[m\times 1]}{\mathbf{g}_Z} = \underset{[m\times n]}{\Psi}\,\underset{[n\times 1]}{\boldsymbol{\rho}} \tag{2.22}$$

This formulation of the interpretation problem changes the total number of unknowns. If they are less than observation, namely $m > n$, least-square can be used to carry out a solution. This is not simple as it seems. In fact there are the two well known problems already described: nonuniqueness and instability of the solution. The reason for the instability can be seen from simple algebraic considerations. Each

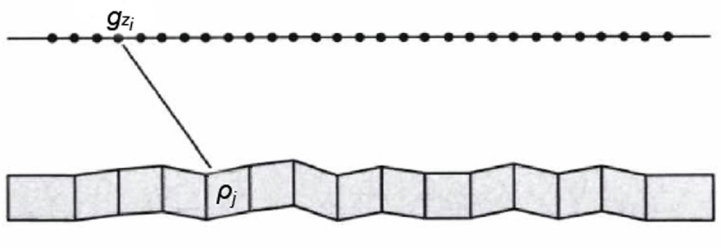

Figure 2.9: Effect of cell j on the observation i

column of matrix Ψ represents the total-field anomaly along a profile over a single cell, namely, cell j. If cell widths are small relative to depth, then the profile over single cell j will be very similar to profiles over cell $j+1$ or cell $j-1$. In other words, small cell width causes neighbouring columns of matrix ψ_{ij} to be similar. In the parlance of matrix algebra, the matrix becomes ill conditioned. To see how this situation might affect solutions for ρ_j, consider just two simultaneous equations,

$$\begin{cases} z_1 = a_{11}x + a_{12}y \\ z_2 = a_{21}x + a_{22}y \end{cases} \tag{2.23}$$

representing some experiment, such as a simple case of equation 4.3; z_1 and z_2 are measured quantities, a_{11}, a_{12}, a_{21}, and a_{22}, are calculated quantities, and x and y are to be determined. As shown in figure 2.10, these two equations define lines in x, y space, and the solution (x_0, y_0) of the two equations is given by the intersection of the two lines. Errors in measurements of z_1 or z_2 cause parallel displacement of the lines. If the lines make a large angle with each other, as depicted in figure 2.10(a), slight displacements will not greatly affect the determination of (x_0, y_0). However, if the two lines are nearly parallel (see figure 2.10(b)), slight errors in z_1 or z_2 will cause significant errors in the determination of (x_0, y_0), and the solution is unstable.

The two lines will be nearly parallel if $a_{11}/a_{12} \approx a_{21}/a_{22}$. In terms of the magnetic layer (Figure 10.1), this kind of situation would occur if the field at point i due to

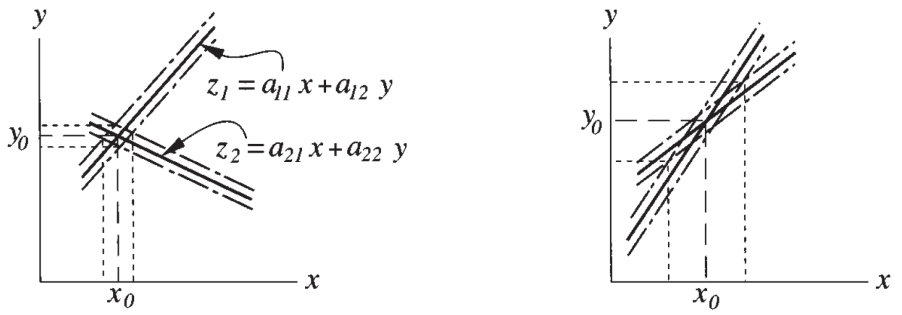

(a) The two solid lines make a large angle to each other, small errors in z_1 or z_2 will not affect the solution greatly

(b) The two lines are nearly parallel, small errors in z_1 or z_2 will greatly affect the solution

Figure 2.10: Solution of two simultaneous equations. Equations are represented by solid lines and solution (x_0, y_0) is shown by their intersection. Errors in z_1 or z_2 cause lines to shift up or down, as shown by dashed-dotted lines (Blackely, 1996)

cell j is similar to the field at point i due to cell $j+1$ and if the field at point i due to cell j is similar to the field at point $i+1$ due to cell j. Equation 10.8 is simply an N-dimensional extension of these two simultaneous equations. Rows and columns of Ψ are smoothly varying functions. Hence, the forward calculation of g_{Z_i} from ρ_j is a smoothing operation, whereas the inverse calculation is an unsmoothing operation. Moreover, the deeper the layer is relative to cell width, the smoother is the matrix Ψ. If cell width is too small relative to the depth to the layer, the matrix Ψ becomes ill-conditioned, and small changes in will cause unrealistic values in the calculated ρ_j. To avoid the ill-conditioning there are basically two ways: the first is to reduce resolution, obviously losing in quality of the interpretation; the second is to apply one of the technique seen in section 2.2. Further details are reported in Blackely (1996).

2.4.2 Nonlinear inverse problem

The potential field on the left side of equation 2.2 and 2.18 is a linear functional of the distribution of mass. In fact, doubling the mass density doubles the amplitude of the total-field anomaly, whereas tripling the mass density would triple the amplitude of the anomaly. In general terms, a system is said to be linear if it satisfies the following test: if $f_1(P)$ is the field caused by source distribution $s_1(Q)$, and $f_2(P)$ is the field caused by another distribution $f_2(Q)$, then the field caused by $as_1(Q) + bs_2(Q)$ is simply $af_1(P) + bf_2(P)$, where a and b are constants.

The same cannot be said for the other parameters that define the source. The gravity field is not a linear functional of, for example, depth, thickness, or shape of the source. All these parameters are contained within $\psi\,(P, Q)$ and in the limits of integration implied by volume v_Q. Inverse methods that attempt to estimate these nonlinear parameters are called nonlinear methods. It should be noted that nonlinear methods usually entail simplifying assumptions that in effect linearize the problem.

Mainly, what it is possible to study is a characteristic of geometry, under some fixed hypothesis, in order to remove the ill-conditioning of the resolution system. Thus it's possible to estimate parameters such as the shape of the source (Fedi and Abbas, 2013; Corbató, 1965) or its depth . The other possibility is the use of ideal body theory (Parker, 1974, 1975).

2.5 Geological information

In the previous sections the need for a-priori information in order to reduce the solutions domain was highlighted. Sampietro and Sansó (2012) showed that in order to get unique solution some constrains on density or geometry of the anomaly source are necessary. A good starting point for the building of those constrains is the geological information available for the area under investigation.

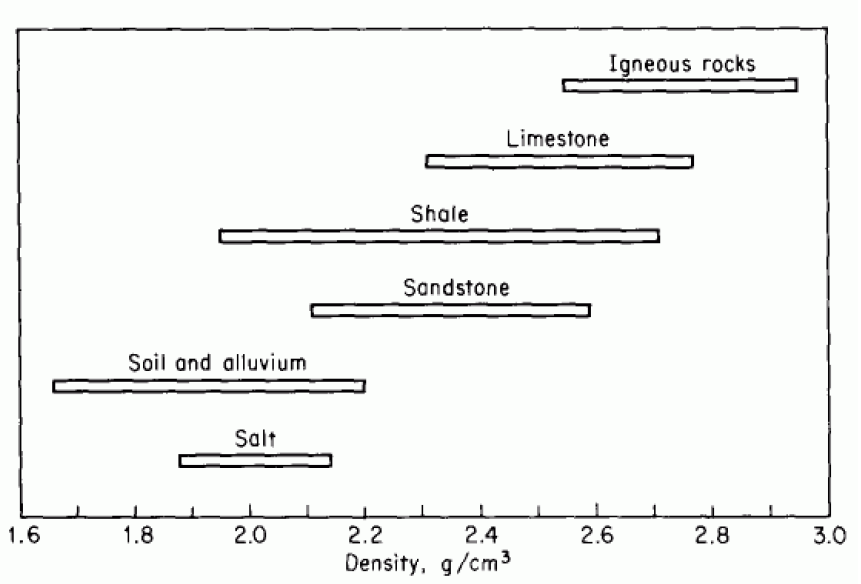

Figure 2.11: Table of density range for some lithotype

In particular, geological data are often qualitative and based on rock outcrops, core drilling, on the historical knowledge of the place, or from shallow geophysical prospection. Clearly at the base of this process there is geologist experience. The results is a vertical cross-section of the subsurface, where the various geological materials are depicted. Obviously the border are hypothetical and they may be large approximation of the reality. An example of cross section is shown in figure 2.12. To give the complete dataset about the place also the average density of each materials can be found in geological literature. In fact it's common to find table like the one represented in figure 2.11 (see Christensen and Mooney 1995), where for each lithology the range of possible density is represented. Essentially, it is derived from the collection of results of surveys all along the planet.

Whenever geological information seems imprecise and inadequate it is very useful to introduce a solid starting point in gravity field interpretations. In fact it introduces during the inversion process an information that is representative of the investigated

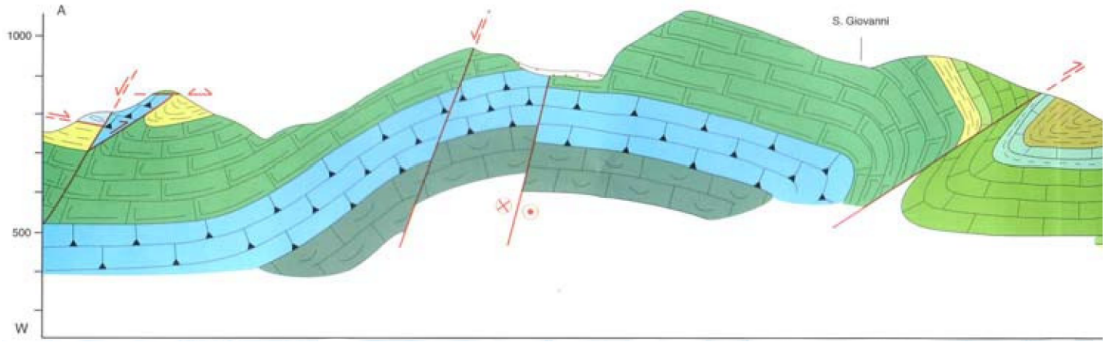

Figure 2.12: Example of geological section

place and can be helpful to design a blurred and sharpened initial model in a trial-error solution or to add constrains in inverse problem solution.

In hydrocarbon exploration it's common to joint seismic with gravity prospections, especially in case of salt dome. In fact salt dome are one of the most important geological structure near which oil may remain trapped. It happens especially in the deeper portion of the dome, but seismic prospection are not able to recover a resolute and precise image of this portion of the structure, due to salt elastic characteristics. A typical situation is shown in figure 2.13, where it's visible that the position of the oil traps is in the blurred and sharpened zone of the seismic profile.

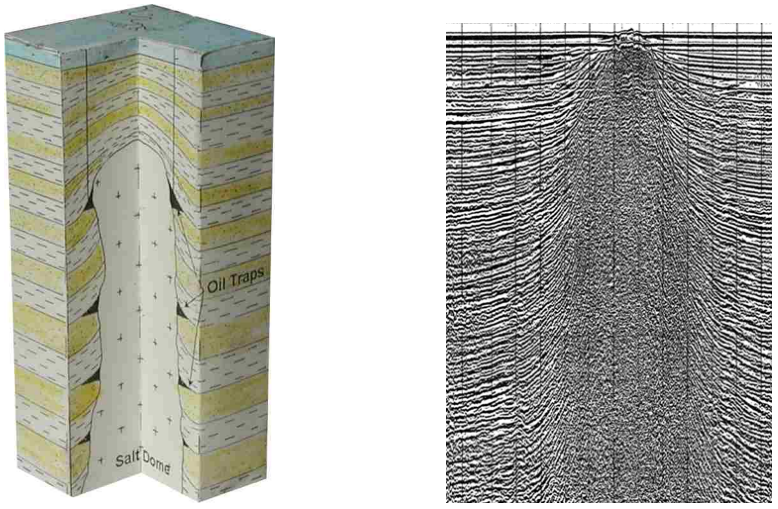

Figure 2.13: Example of seismic section of a salt dome

Chapter 3

Bayesian approach to geophysical inversion problems

The proposed inversion method has the aim to integrate gravity observations with the geological information. As already seen, the main difficult comes from the fact that the first is a quantitative data, with its well known problems of instability and uniqueness in the solution, while the second is only qualitative information. The bayesian approach allows to connect the two dataset using statistical inference (Press, 1968; Wiggins, 1969; Jackson and Matsu'ura, 1985; Mosegaard and Tarantola, 1995; Mosegaard et al., 1997; Tarantola, 2002). More in general the media properties, e.g. elastic or electrical properties or density in gravity case are linked with the information carried by geology, namely a categorical variable, like the lithotype, Thus a relation between primary model parameters space and secondary model space is provided by petrophyisics, geostatistics, or geology correlation (see figure 3.1). The mathematical framework used requires the representation of the information by probability density functions (*pdf*), defined over the space of model parameters. The final outcome, after the combination of model spaces and data space is the posterior *pdf*. In the current chapter the theoretical and mathematical formulation of the bayesian approach will be illustrated. A detailed discussion the reader can refer to Bosch (1999) or Geman and Geman (1984).

In principle, the media properties can be represented by continuous field defined over the investigated volume. Nevertheless, the inference of these function involves an infinite dimensional problem that is difficult to manage. The common approach in this cases, as seen in chapter 2, is to discretize this continuous fields, such that the infinite dimension field inference problem is translated into a finite dimensional space. The formal description of the properties within the investigated volume Ω follows the parametric model $\mathbf{z}_i(\mathbf{r}, \mathbf{m_i})$ to describe the generic ith properties as function of a finite set of parameters $\mathbf{m_i}$ and of the position $\mathbf{r} \in \Omega$. The field can be modelled using basically three methods:

1. a set of blocks, where each one as an assigned value to describe the whole field, thus become a piecewise constant function;
2. a set of point in Ω with assigned value that are combined with an interpolation rule, in order to recover the information in the whole space;

3. linear combination of bases function.

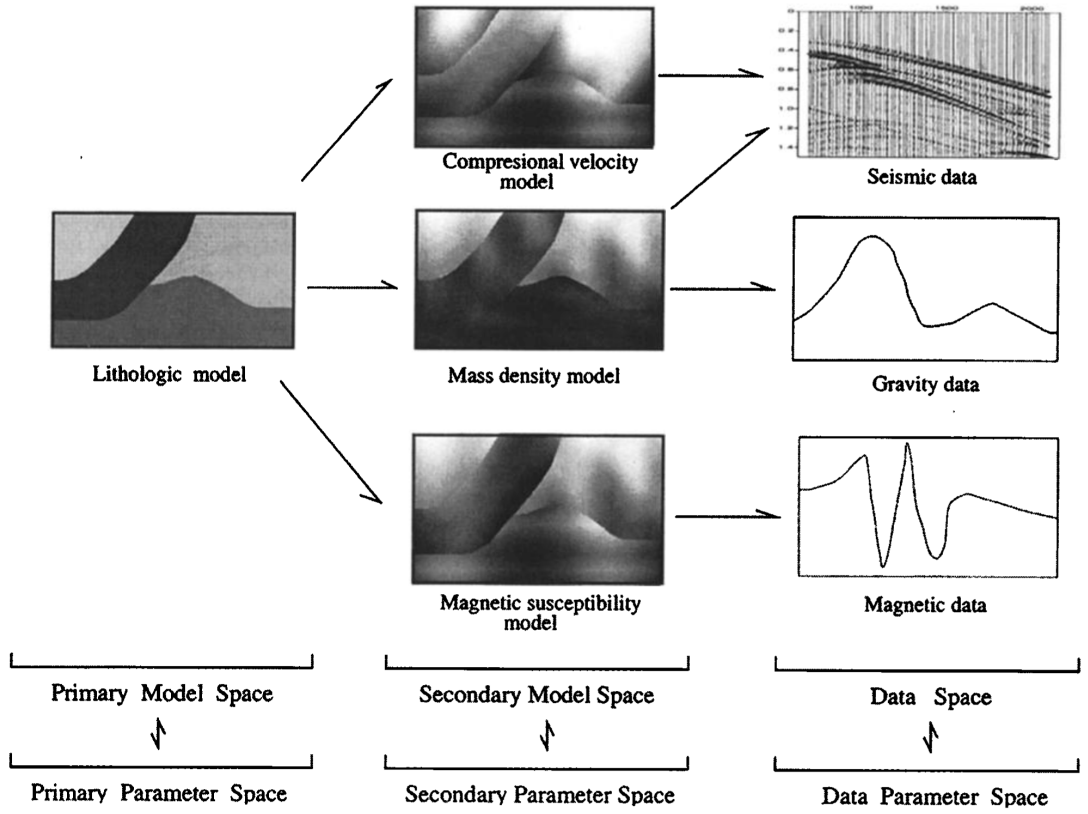

Figure 3.1: Parameters spaces and models spaces in the multiple property geophysical problem. The link between the primary and secondary model space is provided by the petrophysical and the geostatistical information. The link between the secondary models space and the data space is established by the forward geophysical calculation. The arrows indicate the forward direction from the primary model to the data space (Bosch, 1999).

In the general formulation of the problem a series of physical and geological characteristic of the lithological material is considered. The array $\mathbf{z}$ and $\mathbf{m}$ become as many as the number of modelled physical quantity. Hence – calling the model parameter space $\mathcal{M}_i$ the space containing the array of the model parameters $\mathbf{m}_i$, and the property model space $\mathcal{Z}_i$ the space containing the property of fields calculated from the parameters – the joint parametrization requires a joint model parameter space, namely the product space $\mathcal{M} = \mathcal{M}_1 \times \mathcal{M}_2 \times \cdots \times \mathcal{M}_k$, and the joint model space being $\mathcal{Z} = \mathcal{Z}_1 \times \mathcal{Z}_2 \times \cdots \times \mathcal{Z}_k$. The distinction is important in this work because the property field ($\mathcal{Z}$) is directly derived from the a-priori information and it has to be transformed in prior information on the model parameters, that is physical characteristics or, in other words, the secondary model space. The joint spaces $\mathcal{M}$ and $\mathcal{Z}$ are also indicated with the notation $\mathbf{m} = \{\mathbf{m}_1, \mathbf{m}_2, \cdots, \mathbf{m}_k\}$ for the joint model parameters array and $\mathbf{z}(\mathbf{m}, \mathbf{r}) = \{\mathbf{z}_1(\mathbf{m}_1, \mathbf{r}), \mathbf{z}_2(\mathbf{m}_2, \mathbf{r}), \cdots, \mathbf{z}_k(\mathbf{m}_k, \mathbf{r})\}$ in case of the joint property model; each individual $\mathbf{z}_i(\mathbf{m}_i, \mathbf{r})$ is called a property model.

The bayesian approach formulates the inversion problem as an inference problem. It consist of updating the prior knowledge of the models (in this work the lithology

and the density), using the results collected with geophysical surveying experience. In the current work only gravity surveying is used, but for a general formalization of the problem is better to consider a series of geophysical methods. The inference problem is formulated in the joint model parameters space $\mathcal{M}$, where the known information is expressed by a *pdf*. Thereafter, the initial state of the inference problem is described by a prior probability density $\rho(\mathbf{m}_1, \mathbf{m}_2, \cdots, \mathbf{m}_k)$ and the updated state by the posterior probability density $\sigma(\mathbf{m}_1, \mathbf{m}_2, \cdots, \mathbf{m}_k)$, which is obtained as (Tarantola, 2002; Tarantola and Valette, 1982):

$$\sigma(\mathbf{m}_1, \mathbf{m}_2, \cdots, \mathbf{m}_k) = c\ \rho(\mathbf{m}_1, \mathbf{m}_2, \cdots, \mathbf{m}_k)\ \mathcal{L}(\mathbf{m}_1, \mathbf{m}_2, \cdots, \mathbf{m}_k) \tag{3.1}$$

where $\mathcal{L}(\mathbf{m}_1, \mathbf{m}_2, \cdots, \mathbf{m}_k)$ is the likelihood function and c a normalization constant. The likelihood function measures the misfit between the modelled geophysical signal, in the specific case the chosen forward gravity model, and the observations. In the next sections it will be discussed the structure of the prior density, likelihood function and posterior probability.

3.1 The prior probability density

The prior probability density function represents the prior knowledge about model properties at individual positions, spatial relations of property values, cross-relation between different properties, and spatial dependence of cross-relations. As a consequence, it is a complicated function and it is difficult to formulate directly into the joint model space. The simplest way to deduce it is to decompose the whole probability density function into two or more convenient factors using the rule of conditioned probability, derived from the so-called Bayes' theorem (Bayes, 1984):

$$\rho(\mathbf{m}_1, \cdots, \mathbf{m}_k) = \theta_{s|p}(\mathbf{m}_1, \cdots, \mathbf{m}_k | \mathbf{m}_1, \cdots, \mathbf{m}_n)\ \rho_p(\mathbf{m}_1, \cdots, \mathbf{m}_n) \tag{3.2}$$

Now on, the considered partition of the model space is the division between primary and secondary properties. The first is represented by term $\mathcal{M}_{pri} = \mathcal{M}_1 \times \cdots \times \mathcal{M}_n$, while the second by $\mathcal{M}_{sec} = \mathcal{M}_{n+1} \times \cdots \times \mathcal{M}_k$. Therefore, ρ_p is the term containing the information about the primary media properties, namely a marginal density, and $\theta_{s|p}$ is a conditional probability distribution that contains knowledge about the secondary properties and their relation with primary ones. This inference strategy in the current inversion problem has the following advantages:

1. there are often some privileged properties better related with the structure of the media and more relevant to the determination of the rest of the properties. Primary simulation of this property is needed to simulate the rest of them (Deutsch and Journel, 1992);
2. the conditional probability density is particular convenient to introduce petrophysical law (empirical or theoretical) relating rock properties together. On the other hand, the marginal probability density is useful to describe the properties better constrained by prior knowledge.

These advantages are particular relevant when lithology is used as primary properties. In fact all the other physical rock properties used in geophysical calculation,

that is for the current work the mass density, are strongly dependent from it, because they are macroscopical characteristics related to the structure of the rock, namely its lithology.

Depending on the properties information available, this principle of decomposition could be applied against at the various subspace. Thus, there is a larger partition of the model space, and the prior probability density function become simpler to be formalized. The other important assumption usually done is the statistical homogeneity, namely the fact that the conditional probability density functions do not change within the space. This hypothesis means that taking, as usual, the lithology as primary parameters and considering a class, its relation with its secondary properties (like the mass density) is the same, independently from its position in the studied volume Ω.

3.2 The likelihood function

In a general formulation of the problem, consider m different geophysical methods used to explore the studied region (see figure 3.1) and the data parameters array $\mathbf{d}_1, \mathbf{d}_2, \cdots, \mathbf{d}_m$ that describes the observation of each used surveying technique. The joint data parameter space become the product of the spaces of each considered method, that is $\mathcal{D} = \mathcal{D}_1 \times \mathcal{D}_2 \times \cdots \times \mathcal{D}_m$. The information so provided is described by a joint probability distribution $\nu(\mathbf{d}_1, \cdots \mathbf{d}_m)$ defined over the joint data space, with a product structure, on the base of the assumption of observation independence between different geophysical methods.

$$\nu(\mathbf{d}_1, \cdots \mathbf{d}_m) = \prod_{i=1}^{m} \nu_i(\mathbf{d}_i) \tag{3.3}$$

Furthermore, the ith geophysical forward problem is assumed to be solved exactly, that is a forward solution can be computed. It is represented by a function $\mathbf{d}_i^{cal} = \mathbf{g}_i(\mathbf{m}_1, \cdots, \mathbf{m}_k)$, for the whole set of observation techniques. Each of the method is defined on the joint space of parameters $\mathcal{M}$, even if each one use only its related parameter (e.g. gravity use mass density). Finally, the likelihood function become:

$$\mathcal{L}(\mathbf{m}_1, \cdots, \mathbf{m}_k) = \nu(\mathbf{g}_1(\mathbf{m}_1, \cdots, \mathbf{m}_k), \cdots \mathbf{g}_m(\mathbf{m}_1, \cdots, \mathbf{m}_k)) \tag{3.4}$$

Thanks to the assumption of statistical independence between uncertainness of the various geophysical methods the joint likelihood is the product of the single likelihood. Hence, equation 3.4 become:

$$\mathcal{L}(\mathbf{m}_1, \cdots, \mathbf{m}_k) = \prod_{i=1}^{m} \nu(\mathbf{g}_i(\mathbf{m}_1, \cdots, \mathbf{m}_k)) = \prod_{i=1}^{m} \mathcal{L}(\mathbf{m}_1, \cdots, \mathbf{m}_k) \tag{3.5}$$

This hypothesis of independence of the observational uncertainties across the different surveying techniques is realistic in most of the cases. In fact sources of errors affecting the different geophysical data (e.g. instrumental, environment, human, etc.) are commonly different between all the methods.

3.3 The posterior probability density

Summarizing the results of previous sections, the posterior probability density function can be calculated. In particular, combining equations 3.1, 3.2, 3.5 the posterior *pdf* is expressed as:

$$\sigma\left(\mathbf{m}_{pri}, \mathbf{m}_{sec}\right) = \underbrace{\theta_{s|p}\left(\mathbf{m}_{pri}|\mathbf{m}_{sec}\right)\ \rho_p\left(\mathbf{m}_{pri}\right)}_{\rho(\mathbf{m}_{pri},\mathbf{m}_{pri})} \underbrace{\prod_{i=1}^{m} \mathcal{L}_i\left(\mathbf{m}_{pri}, \mathbf{m}_{pri}\right)}_{\mathcal{L}(\mathbf{m}_{pri},\mathbf{m}_{pri})} \tag{3.6}$$

where $\mathbf{m}_{pri}$ denotes the array $\{\mathbf{m}_1, \cdots, \mathbf{m}_n\}$ of primary model parameters and $\mathbf{m}_{sec}$ the array $\{\mathbf{m}_{n+1}, \cdots, \mathbf{m}_k\}$ of secondary model parameters. The likelihood $\mathcal{L}_i\left(\mathbf{m}_{pri}, \mathbf{m}_{sec}\right)$ function is defined over the joint model space to keep generality, but in the studied case, as usual, it depends only from secondary parameters, because primary model parameters are associated to the lithology.

The integration of the joint posterior density over the secondary parameters space gives the marginal posterior density for primary parameters:

$$\sigma_p\left(\mathbf{m}_{pri}\right) = c\ \rho_p\left(\mathbf{m}_{pri}\right) \int_{\mathcal{M}_{sec}} \theta_{s|p}\left(\mathbf{m}_{pri}|\mathbf{m}_{sec}\right) \prod_{i=1}^{m} \mathcal{L}_i\left(\mathbf{m}_{pri}|\mathbf{m}_{sec}\right)\ d\mathbf{m}_{sec} \tag{3.7}$$

where the integral term is the likelihood function for the primary model parameters. To estimate the final value of the model parameters there are basically two approaches: the first is to sample the posterior *pdf*, while the second is to find its maximum, for example using a gradient method or another optimization method. This second approach is accettable only if the posterior *pdf* is a monomodal, because it provides an incomplete representation, that may be wrong in case of complex shapes, being multimodal. In fact, the posterior *pdf* of multiple-data multiple-parameters inverse problem results from the combination of several nonlinear geophysical simulations and complicated priors and it is likely to be complicated function. Although the sampling approach requires larger calculation effort than the optimization approach, it will be the general method that provides more information about the posterior knowledge of the studied volume. However, in the current job the chose approach is the maximum of the posterior. To avoid the problem of a classical maximization approach like the gradient one, a simulated annealing aided by the Gibbs sampler is used (Sansò et al., 2011). In fact it is demonstrated that it provides the global minimum if the temperature parameters decrease sufficiently slow, thus the problem of complex shape of multimodal posterior *pdfs* is solved and, respect to a sampling solution approach, it requires less time.

3.4 Problem formalization

We shall apply Bayes' theorem in the usual form (Bayes, 1984; Box and Tiao, 2011):

$$P\left(\mathbf{x}|\mathbf{y}\right) \propto \mathcal{L}\left(\mathbf{y}|\mathbf{x}\right) P\left(\mathbf{x}\right) \tag{3.8}$$

where $\mathbf{y}$ is a vector of observable quantities, while $\mathbf{x}$ is a vector of body parameters. The body B is split into voxels, V_i, with index $i = 1, 2, ..., N$; each voxel will carry two parameters (ρ_i, L_i) where ρ_i is the mass density in the voxel and L_i is a label variable attributing to V_i the presence of a certain geological unit chosen from an a-priori archive, e.g. water, sediment, salt, rock of a given type, etc. So ρ_i is a continuous variable and L_i a discrete one among the M integers denoting the various materials.

Crucial is the way in which the prior information is supplied, namely the shape of $P(\mathbf{x}) = P(L_1, \rho_1; L_2, \rho_2; ...; L_N, \rho_N)$. We assume that:

$$P(\mathbf{x}) = \prod_i P(\rho_i|L_i) \cdot P(L_1, L_2, ..., L_N) \tag{3.9}$$

meaning that, once a label $L_i = \ell$ has been chosen for V_i, the corresponding density will follow the law $P(\rho_i|L_i)$, which in our case is just a normal distribution:

$$P(\rho_i|L_i) \sim \mathcal{N}\left(\overline{\rho}_\ell, \sigma_\ell^2\right) \tag{3.10}$$

with the mean $\overline{\rho}_\ell$ and the variance σ_ℓ^2 given by geological tables. In this respect a comprehensive set of rocks properties can be found for instance in Christensen and Mooney (1995). As for the prior $P(\mathbf{L}) \equiv P(L_1, L_2, ..., L_N)$ we assume to have a Gibbs distribution (Azencott, 1988):

$$P(\mathbf{L}) = e^{-\mathcal{E}(\mathbf{L})}, \tag{3.11}$$

where the energy $\mathcal{E}(\mathbf{L})$ depends only on values ℓ_i^o of L_i provided by the prior model, as well as from cliques of order two expressing the fact that the value of L_i is more likely to be equal to the value of the labels of nearest neighbour voxels according to the following rules:

$$P(L_i = \ell|\mathbf{L}_{\Delta i}) \propto e^{-\gamma s^2\left(L_i, \ell_i^o\right) - \lambda \sum_{j \in \Delta_i} q^2(L_i, L_j)} \tag{3.12}$$

where γ, λ are parameters to be tuned, and

$$s^2(L_i, \ell_i^o) = \begin{cases} 0 & \text{if } L_i = \ell_i^o \\ \alpha_k & \text{if } L_i = k \neq \ell_i^o \end{cases} \tag{3.13}$$

$$q^2(L_i, L_j) = \begin{cases} a & \text{if } L_i = L_j \\ a_j & \text{if } L_i \neq L_j \end{cases}, \tag{3.14}$$

with $V_j \in \Delta_i$ and Δ_i is the neighbourhood of the voxel V_i, depicted in figure 3.2 in a 3D case.

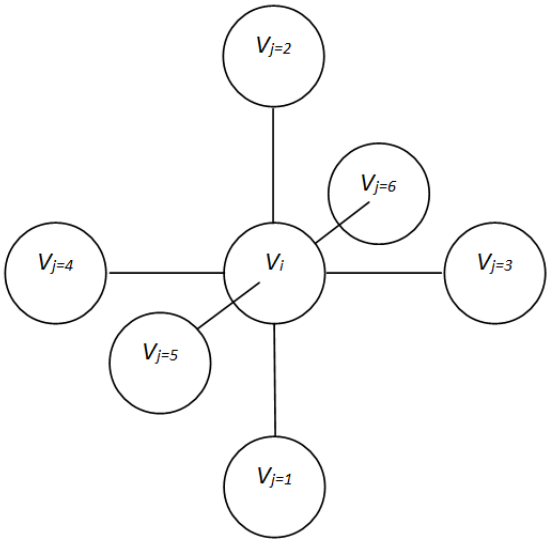

Figure 3.2: Definition of the neighbourhood Δ_i of the voxel V_i

Note that by tuning α_k and a, a_j one can create a hierarchy of values most probable for L_i, thus implementing an a-priori table of proximity of geological units. For example supposing to have three units, $\ell = \{1, 2, 3\}$, and a proximity table as the one presented in figure 3.3, this translates into the following definition:

$$s^2 = \begin{cases} 0 & \text{if } L_i = \ell_i^o \\ \alpha & \text{if } L_i \text{ is a } 1^{st} \text{ neighbour of } \ell_i^o \\ \beta & \text{if } L_i \text{ is a } 2^{nd} \text{ neighbour of } \ell_i^o \end{cases}, \tag{3.15}$$

$$q_j^2 = \begin{cases} a & \text{if } L_i = L_j \\ b & \text{if } L_i \text{ is a } 1^{st} \text{ neighbour of } L_j \\ c & \text{if } L_i \text{ is a } 2^{nd} \text{ neighbour of } L_j \end{cases} \tag{3.16}$$

with $\beta > \alpha > 0$ and $c > b > a$.

	1	2	3
1	X	X	
2	X	X	X
3		X	X

Figure 3.3: Example of proximity table. The geological unit 1 can be close to unit 2 but not to unit 3

Two remarks are in order: the first is that $\mathbf{L}$, with prior $P(\mathbf{L})$, is indeed a Markov random field (MRF, see Rozanov 1982). The second is that the final result of our

optimization will depend a lot from the chosen values of all the constants, which have to be tuned on the specific example by hand.

As always for a MRF, the characteristics, that is the conditional distributions depicted in equation 3.12, determine a joint distribution $P(\mathbf{L})$ such that:

$$\log P(\mathbf{L}) \propto -\gamma \sum_i s^2(L_i, \ell_{oi}) - \lambda \sum_i \sum_{j \in \Delta_i} q^2(L_i, L_j). \tag{3.17}$$

Summarizing, the logarithm of the posterior distribution, shown in equation 3.8, will be written as:

$$\begin{aligned} L(\mathbf{x}) = L(\boldsymbol{\rho},\ \mathbf{L}\ ) = \log P(\mathbf{x}|\mathbf{y}) = -\frac{1}{2}(\boldsymbol{\Delta g} - A\boldsymbol{\rho})^T \boldsymbol{C}_{\boldsymbol{\Delta g}}^{-\mathbf{1}}(\boldsymbol{\Delta g} - A\boldsymbol{\rho}) + \\ -\frac{1}{2}(\boldsymbol{\rho} - \overline{\boldsymbol{\rho}})^T \boldsymbol{C}_{\boldsymbol{\rho}}^{-\mathbf{1}}(\boldsymbol{\rho} - \overline{\boldsymbol{\rho}}) - \frac{1}{2}\gamma \sum_i \mathbf{s}^2(\ell_i, \ell_i^o) - \lambda \sum_i \sum_{j \in \Delta_i} \mathbf{q}^2(\ell_i, \ell_j) \end{aligned} \tag{3.18}$$

where we recall that $\boldsymbol{\Delta g}$ is the vector of observed gravity anomalies, $\boldsymbol{C}_{\boldsymbol{\Delta g}}$ the covariance matrix of their noise assumed here to be diagonal, A is the forward modelling operator from densities to gravity anomalies, $\boldsymbol{\rho}$ and $\overline{\boldsymbol{\rho}}$ the vectors of components ρ_i and $\overline{\rho}_i = \overline{\rho}(\ell_i)$, $\boldsymbol{C}_{\boldsymbol{\rho}}$ the corresponding covariance matrix and s^2, q^2 given by equations 3.13 and 3.14. This is the target function we want to maximize with respect to ρ_i and L_i.

Chapter 4

Solution strategies

The aim of this work, as already seen, is to integrate geological information with the gravity observation. To give a weight to the geology the bayesian approach, described in the previous chapter, is used. In the current chapter the solution algorithm will be detailed explained.

To reach the final solution at the inverse gravimetric problem using the bayesian approach well described in section 3.4 the goal is to maximize the posterior probability density function, or as shown in equation 3.16 its logarithm. Clearly, the maximization problem becomes a minimization one if the sign in front of the equation is changed, thus the problem is translated into the minimization of the opposite of the logarithm of the posterior density function respect to the parameter vectors $\mathbf{L}$ and $\boldsymbol{\rho}$. The final formulation of the problem become:

$$\min_{\mathbf{L},\boldsymbol{\rho}} \quad \{-L(\boldsymbol{\rho},\ \mathbf{L}\ )\} = \min_{\mathbf{L},\boldsymbol{\rho}} \quad \left\{ (\boldsymbol{\Delta g} - A\boldsymbol{\rho})^T \boldsymbol{C}_{\boldsymbol{\Delta g}}^{-\mathbf{1}} (\boldsymbol{\Delta g} - A\boldsymbol{\rho}) + \right.$$
$$\left. + (\boldsymbol{\rho} - \overline{\boldsymbol{\rho}})^T \boldsymbol{C}_{\boldsymbol{\rho}}^{-\mathbf{1}} (\boldsymbol{\rho} - \overline{\boldsymbol{\rho}}) + \gamma \sum_i \mathbf{s}^2(\ell_i, \ell_i^o) - \lambda \sum_i \sum_{j \in \Delta_i} \mathbf{q}^2(\ell_i, \ell_j) \right\} \quad (4.1)$$

The big issue is how to deal with this problem, because of, to guarantee a good result the absolute minimum must be found. The proposed solution is based on the simulated annealing. Due to the nature of the geometrical relation existing inside the voxels distribution the investigated volume is well described with a Markov Random Field (MRF), thus the simulated annealing can be carried out with the aid of a Gibbs Sampler.

Basically, two different strategies based on the simulated annealing are pursued during the project development, in order to become able to deal with discrete and continuous variables like label ($\mathbf{L}$) and density ($\boldsymbol{\rho}$) involved in the solution:

1. the first approach is to give an iteratively estimation of the density derived from a least square adjustment constrained with the mean value of the density associated to the chosen label, and of the labels using the simulated annealing once density are fixed;
2. discretize the value of density near its average value, in order to give a series of discrete possible solution, each one with a different a-priori *pdf*. Now it's possible to find the solution only with simulated annealing aided by the Gibbs sampler

The first strategy had some problems due to the fact that in the mixed approach to the minimization optimization it is not possible to maintain coherency between least square and simulated annealing. In fact at each iteration there is a change of the covariance matrix of densities, used as regularizator in LS. That fact implies that the objective function in not the same at every iteration, thus the minimum is impossible to find. Hence, in the follow paragraphs only the second approach is discussed, after a rough description of Gibbs sampler and simulated annealing optimization techniques and of the used forward model.

4.1 Geometric model

To apply the algorithm just described the concept of voxel is introduced. It means that the volume is described by the sum of a discrete number of cells. As already seen, this is a common method to model the investigated space, often used in inverse problems. The developed solution is based on a planar approximation. Each voxel is described by a series of regular rectangular prism. Obviously, this is not the only solution possible, but is the simpler to implement during the testing phase of the algorithm, done with simulated data.

The vertical gravity signal of each prism is modelled with the formulation derived in equation 2.8 (Nagy et al., 2000), here reported:

$$g_Z(P) = -G\rho \left| \left| \left| x \ln(y+r) + y \ln(x+r) - z \arctan \frac{xy}{zr} \right|_{x_1}^{x_2} \right|_{y_1}^{y_2} \right|_{z_1}^{z_2}$$

recalling that x, y, z are the coordinates difference between the the prism corner and the computational point P. The sign minus depend only on the chosen vertical direction. In this case the z coordinate increase with height. Therefore, the gravity signal of the total studied volume can be obtained simply with the summation of the contribution due to all the N single compartments. Equation 2.8 become:

$$g_Z(P_j) = -G \sum_{i=1}^{N} \rho_i \left| \left| \left| x_j \ln(y_j + r_j) + y_j \ln(x_j + r_j) - z_j \arctan \frac{x_j y_j}{z_j r_j} \right|_{x_{1_j^i}}^{x_{2_j^i}} \right|_{y_{1_j^i}}^{y_{2_j^i}} \right|_{z_{1_j^i}}^{z_{2_j^i}} \tag{4.2}$$

where the term x_j, y_j, z_j, r_j are the coordinates and the euclidean distance expressed in the reference frame with origin in the generic computational point P_j, and their relation with the local coordinate system X, Y, Z used in the plane approximation is:

$$\begin{aligned} x_j &= X - X_{P_j} \\ y_j &= Y - Y_{P_j} \\ z_j &= Z - Z_{P_j} \\ r_j &= \sqrt{\left(X - X_{P_j}\right)^2 + \left(Y - Y_{P_j}\right)^2 + \left(Z - Z_{P_j}\right)^2} \end{aligned}$$

Therefore, the coordinates of the corners of the ith prism referred to the jth computational point are called $x_{1_j^i}$, $x_{2_j^i}$, $y_{1_j^i}$, $y_{2_j^i}$, $z_{1_j^i}$, and $z_{2_j^i}$.

The complete forward model for the chosen geometry is derived combining all the observation on a regular grid and at a constant height. It can be expressed using matrix system. Introducing the term

$$\psi_{ji} = \left\| \left\| x_j \ln\left(y_j + r_j\right) + y_j \ln\left(x_j + r_j\right) - z_j \arctan \frac{x_j y_j}{z_j r_j} \right|_{x_{1_j^i}}^{x_{2_j^i}} \right|_{y_{1_j^i}}^{y_{2_j^i}} \Bigg|_{z_{1_j^i}}^{z_{2_j^i}}$$

to describe the geometric relation between the ith prism and jth computational point the system become:

$$\mathbf{g}_z = A\boldsymbol{\rho} \quad \Rightarrow \quad \begin{bmatrix} g_Z\left(P_1\right) \\ g_Z\left(P_2\right) \\ \vdots \\ g_Z\left(P_j\right) \\ \vdots \\ g_Z\left(P_M\right) \end{bmatrix} = \begin{bmatrix} \psi_{11} & \psi_{12} & \cdots & \psi_{1N} \\ \psi_{21} & \psi_{22} & \cdots & \psi_{2N} \\ \vdots & \vdots & \ddots & \vdots \\ \psi_{j1} & \psi_{j2} & \cdots & \psi_{jN} \\ \vdots & \vdots & \ddots & \vdots \\ \psi_{M1} & \psi_{M2} & \cdots & \psi_{MN} \end{bmatrix} \begin{bmatrix} \rho_1 \\ \rho_2 \\ \vdots \\ \rho_N \end{bmatrix} \tag{4.3}$$

Then, the prisms are associated to the two random variables used in the solution: the label L and the mass density ρ. The probability relation existing between the two is described by a normal distribution (see equation 3.10). The matrix A, once

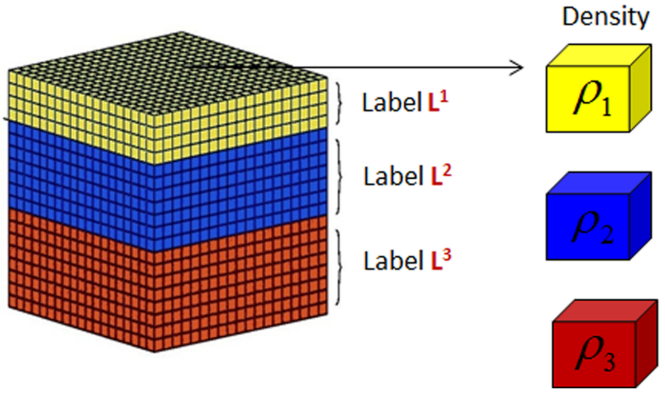

Figure 4.1: The volume is discretized in small prisms, each one associated to a label L and a density ρ

computed is constant during the whole inversion process, because it represent the relation between gravity observation and the density of the cell. The geometry of the problem, namely the subsurface layers, is described by the label assigned to the various voxels, as shown in figure 4.1

4.2 Simulated annealing and Gibbs sampler

Simulated annealing came from the annealing method in physics. This technique was used to increase the size and decrease the number of defects in crystals. This was done by heating and then slowly cooling the crystal. It is an optimization technique used to find the minimum of functions when there are multiple hills and standard hill climbing techniques could trap the algorithm into a local (non global) optimum. Considering a function $\varepsilon(\mathbf{x})$ to minimize in $\mathbf{x} \in Q$, continuous in Q (a close and finite square), where the minimum $E = \epsilon(\bar{\mathbf{x}})$ is reached only in a point $\bar{\mathbf{x}} \in Q$ the family of probability density function

$$f(\mathbf{x}, \lambda) = A_\lambda e^{-\lambda\varepsilon(\mathbf{x})} \tag{4.4}$$

can be written, where the term A_λ is a normalization term

$$A_\lambda^{-1} = \int_Q e^{-\lambda\varepsilon(\mathbf{x})} \tag{4.5}$$

where, according with physical simulation the parameter λ is the inverse of the temperature T, thus the limit $\lambda \to \infty$ correspond to $T \to 0$ and $\lambda \to 0$ correspond to $T \to \infty$. An intuitive description of the is shown in figure 4.2 where $\varepsilon(\mathbf{x})$, $f(\mathbf{x}, \lambda = 0.1)$, $f(\mathbf{x}, \lambda = 10)$ are represented.

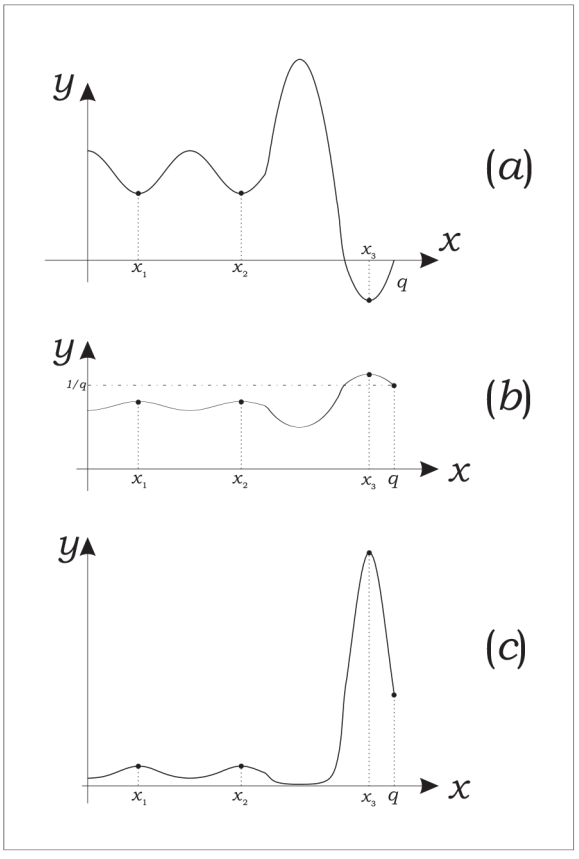

Figure 4.2: Graph of $\varepsilon(\mathbf{x})$, $f(\mathbf{x}, \lambda = 0.1)$, $f(\mathbf{x}, \lambda = 10)$ (Sansò et al., 2011)

Clearly for a small value of λ, namely an higher very value of temperature T, the distribution become a uniform distribution as shown in the follow equation:

$$\lim_{\lambda \to \infty} f(\mathbf{x}, \lambda) = \frac{1}{\mu(Q)}, \mathbf{x} \in Q \tag{4.6}$$

When sampling over the space in the early stages in the algorithm, simulated annealing allows for downhill moves to less optimal values with a certain probability. This allows for jumping out of local maximums. However, as the algorithm progresses the probability of making downhill moves decreases. As a result, one is able to initially sample over a larger space and eventually localize on a maximum, as shown in figure 4.3.

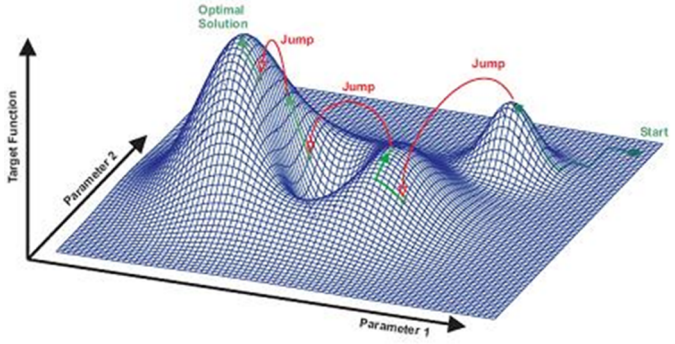

Figure 4.3: Random extractions from the distribution of probability of equation 4.4 by decreasing slowly temperature T (or increasing slowly the parameter λ). The algorithm converge to the global minimum (or maximum)

The difficult arises when sampling the probability distribution of equation 4.4 in case of large quantity of parameters. That's why simulated annealing can be connected to the Gibbs sampling algorithm. In fact Gibbs sampler is particularly appropriate to the sampling of a distribution like 4.4 because such a method require only the knowledge of the conditioned probability distribution of each component x_i respect to the others, that for a MRF is very simple. In fact, it implies only the neighbourhood variables instead of all the variables of $\mathbf{x}$. Hence, once the sequence to sweep all the space is chosen, starting from one of the values $\{x_{0i}\} = \mathbf{x}_0$ at each time one component of $\mathbf{x}$ sampling from the conditioned distributions, where some values are already updated, while the others are the same of the previous step (see figure 4.4). In this way a new vector $\mathbf{x}_1$ is generated and iterating the process we obtain a Markov chain that after a certain time present a probability distribution that is the one shown in equation 4.4.

As already said, in the presented approach to the gravity inversion the two methods are combined. This integration was studied first by Geman and Geman (1984) and consist in the iterative application of Gibbs sampler, in order to pass from $\mathbf{x}_t$ to $\mathbf{x}_{t+1}$, and of simulated annealing, meaning that each iteration the parameter λ is updated in order to pass from λ_t to $\lambda_{t+1} > \lambda_t$. The aim is to obtain for $t \to \infty$ the parameter $\lambda \to \infty$. According to the mechanical similarity the temperature each iteration is update and decreased in order that for $t \to \infty$, the system is frozen, namely $T \to 0$.

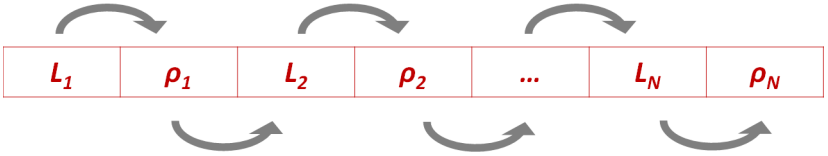

Figure 4.4: Principle of Gibbs sampler to draw samples from a joint distribution of a multidimensional random variable given a proper sequence of its conditional distributions. It requires to order the variables and minimize the function by acting only on a variable at a time.

4.3 Inversion algorithm

The proposed inversion algorithm is developed in its preliminary version using Matlab (Mathworks) programming language. This choice has been done because of its simple interface and matrix management. On the other hand there are some limitations on the quantity of data that is possible to handle. That's why the tests performed in support of the present work, shown in the next chapter, are done with slow resolution.

The final working flux, as shown in figure 4.5, is composed of three main phases:

- An initial phase where data are imported, lithological classes and density intervals are imported and stored. After that it is possible to discretize the density value and associate to each one its prior probability coming from the normal distribution. In this phase the linear operator A of the forward model is computed and stored in order to be used. Furthermore the observation are simulated in a noiseless scenario. The parameters and the constant can be set by the user directly in the code.
- The second phase is the initialization of the simulated annealing algorithm, that is a random initialization of labels. This step correspond to set the temperature T to infinite. Simulated annealing and Gibbs sampler are initialized by seeking in order all the voxels and the value of Gibbs probability (equation 4.4) is computed in each cell for all the possible value of the two variables. A random extraction is performed in order to sample a value for label and density. Once all the voxels are skewed the temperature is reduced according to a law.
- Last step is to determine a convergence criteria. In this case there is only a limitation on the maximum number of iteration and a minimum value of the temperature is set, in order to avoid numerical problems. At the end of the process the results are visualized, typically using vertical cross section.

All the constant are set by hand from the user. Moreover it has some computational time problem. In fact, it needs to be optimized in this respect. In particular, the more time consuming operation is the computation of the forward model, but also the weight due to neighbourhood relationships. Moreover, in order to reduce computational time the other useful improvement to apply is to fix voxels with a posterior probability greater than a threshold (e.g. 95%). In this way the each time a voxel is fixed it does not need more computation, thus is skipped by the routine and finally iteration time decrease rapidly.

However, this is a good starting point to be used in research and development phase of the presented Bayesian approach. Considering the large amount of data, to

develop an optimized version of the software it can be useful to write the software using a low level programming language. Anyway, this is not the aim of the present work.

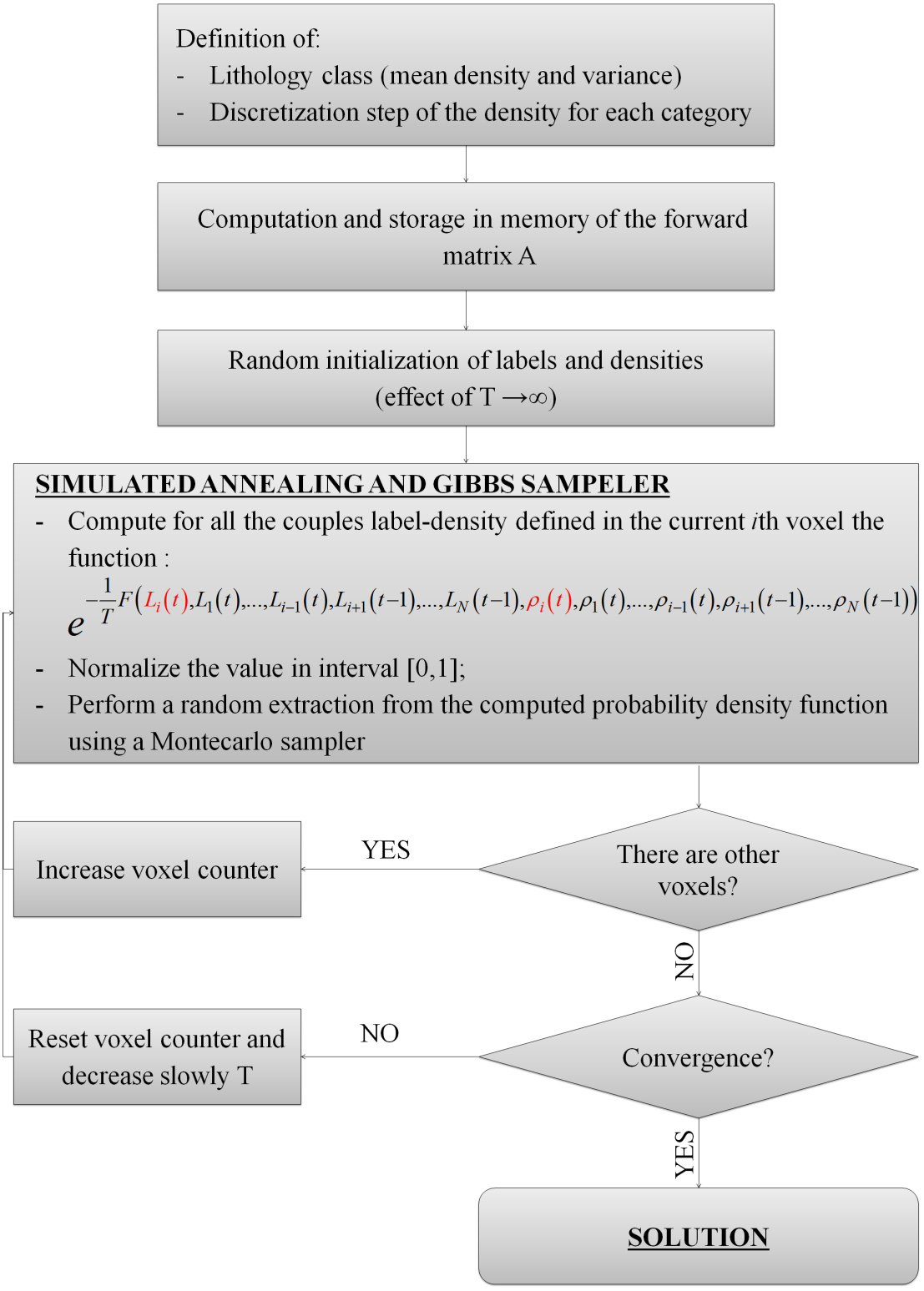

Figure 4.5: Solution algorithm diagram

Chapter 5

Examples

In order to start assessing the effectiveness of the presented Bayesian approach, which is able to consider also qualitative geological information, some simple experiment is carried out. In fact, to allow the computation using common computers high resolution volume discretization cannot be used. The tests consist in recovering the mass density distribution of two 3D synthetic models from their gravitational field.

Moreover, all the observations come from simulated data. In fact, the idea is to compute gravity observation using the forward model, described in previous chapter, on a regular grid, while the geological prior information is derived introducing a small error in the true synthetic model. Finally, the solution can be evaluated on the base of its attitude to recover the true known geological configuration of the original model.

Basically, two test are developed: the first model simulates the recovery of the bathymery, while the second one consists in recovering the shape of a salt dome. The test consists in recovering the mass density distribution of two 3D synthetic models from their gravitational field. In particular the first model simulates the recovery of the bathymery, while the second one consists in recovering the shape of a salt dome. In the bathymetry model only two labels are considered, water and bedrock, defined by $\rho_w = 1000\ kg\,m^{-3}$, $\sigma_w = 30\ kg\,m^{-3}$ and $\rho_b = 2900\ kg\,m^{-3}$, $\sigma_b = 80\ kg\,m^{-3}$ respectively. In the salt dome model three geological units are considered: sediments ($\rho_s = 2200\ kg\,m^{-3}$, $\sigma_s = 40\ kg\,m^{-3}$), salt dome ($\rho_d = 2000\ kg\,m^{-3}$, $\sigma_d = 20\ kg\,m^{-3}$) and the bedrock ($\rho_b = 2900\ kg\,m^{-3}$, $\sigma_b = 80\ kg\,m^{-3}$). In both cases the investigated area is a square of 30 km side and has a depth of 5 km. Furthermore, the models are constant along y direction. This is done in order to simplify data treatment. A vertical cross-section of the synthetic models is represented in figures 5.1(a) and 5.2(a). The volume is modelled by means of 1200 rectangular prisms, each one of dimensions 1.5 *km (x)* $\times$ 5.0 *km (y)* $\times$ 0.5 *km (z)*.

Starting from these models the corresponding gravitational observations are generated by means of Nagy equations (see Nagy 1966) in a noiseless scenario. In particular these observations are generated on a regular grid at an altitude of 500 m and with a spatial resolution of 5 km, thus simulating the result of an aerogravimetric flight. In the follows paragraphs the results of this two simulation are shown and discussed.

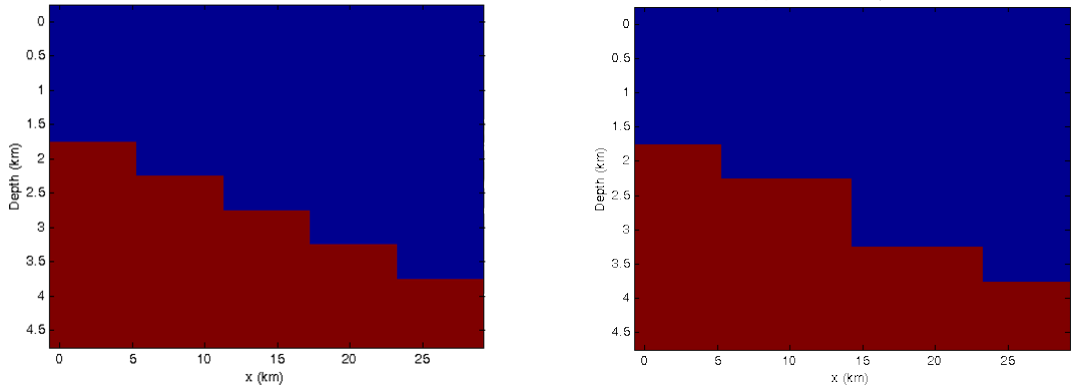

(a) (b)

Figure 5.1: Vertical cross section of the true (a) and a-priori (b) model where blue is water and red bedrock

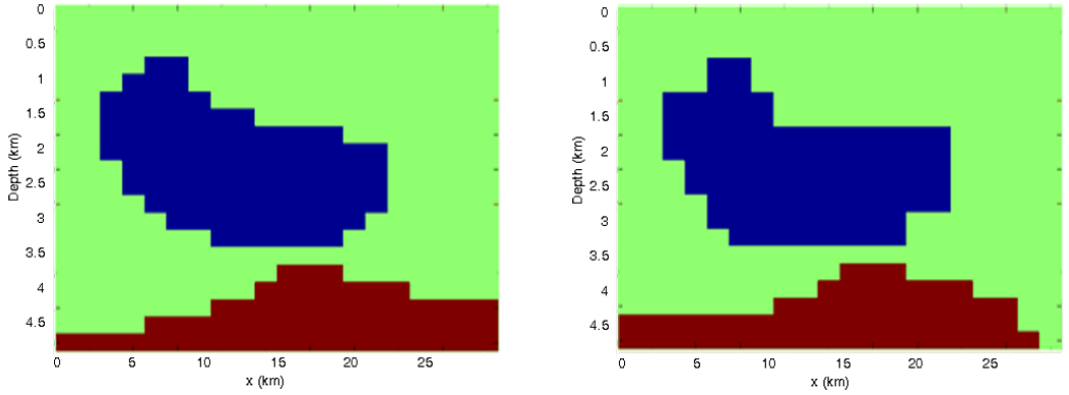

(a) (b)

Figure 5.2: Vertical cross section of the true (a) and a-priori (b) model where blue is the salt dome, green sediments and red bedrock

5.1 Bathimetry: results

The final solution of the example of bathymetry is performed in about 5000 iterations and about 4 hours on a common personal computer. All the cross section of the resulting models in y direction can be seen in figure 5.3. Clearly, they show how the error in the geological model is properly corrected. In fact, 86% of the uncorrect densities and labels are properly corrected. Moreover, there are also error correct voxels that in the final solution change label and density. This problem is emphasized near the edges of studied volume, thus the idea is that it depend mainly from some kind of border effect. On the other hand, increasing the resolution the problem can be limited.

The most time-consuming job was to calibrate the two parameters λ and γ, that are empirically set by end. The presented solution is obtained with their values equal to 0.833 and 0.733 respectively. The other big issue is the temperature range and its decreasing law. In fact from this parameter depend the quality of the final

solution: a fast decreasing law doesn't allow the system to reach a solution, on the contrary if the decrease law is too slow the solution is very time-consuming. Since

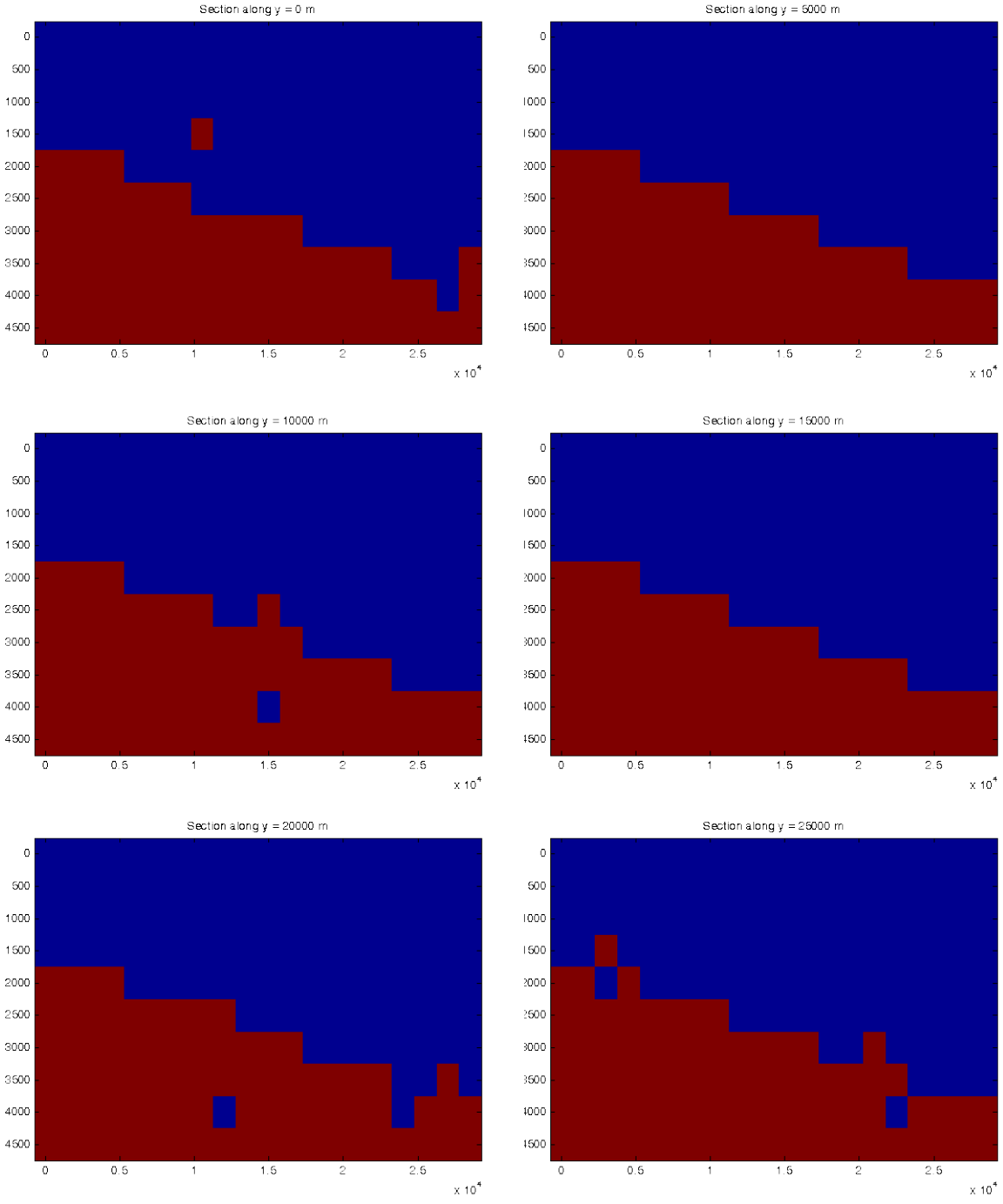

Figure 5.3: Results of Bayesian inversion of the simulated set of data in case of bathimetry (vertical cross-sections)

simulated annealing need to start from a theoretical infinite temperature the values of the labels are random initialized, while this condition represent the sampling from a uniform probability density function.

The Bayesian solution is compared with a standard least squares solution, where the regularization is done on the basis of the geological model and can be seen in figure 5.4. Not being able to modify the labels of voxels the standard least square solution can only fit the observations by changing densities according to the a-priori hypothesis. Clearly the solution is not able to recover possible errors in the a-priori model.

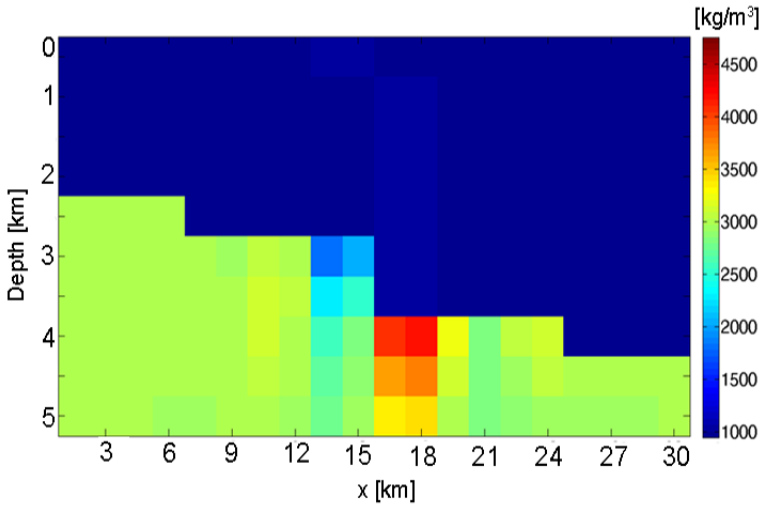

Figure 5.4: Density estimation from classical regularized least squares gravimetric inversion

5.2 Salt dome: results

The results of three layer salt dome interpretation are only partially corrected. In fact only 70% of the uncorrect densities and labels are properly corrected, mainly in the upper part of the subsurface. This is evident in figure 5.5, where one relevant

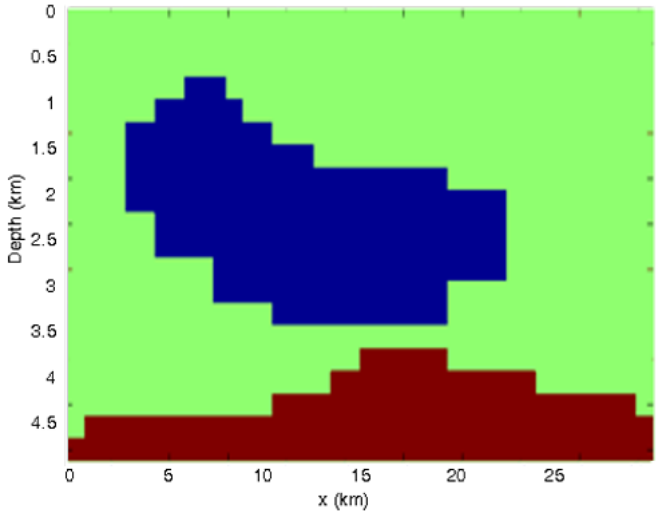

Figure 5.5: Results of Bayesian inversion of the simulated set of data in case of bathimetry (vertical cross-section

section is depicted. The main cause of this problem is the right calibration of all the parameters that plays in the solution algorithm: λ, γ, temperature and its decreasing law. In fact they are all very sensitive to the total number of voxels and their dimensions. In this case probably too high importance is given to geological prior information where gravity signal is weak, i.e. the bottom part of the salt dome.

However, thanks to the quantity of voxels this test requires less computation time than the bathimetry, and only about 1800 iterations. In figure 5.6 it is shown how the residuals between observed and estimated gravity signal converge to a very low acceptable values during algorithm running. Since increasing of iteration means decreasing of the temperature it's clear how at beginning of the process (i.e. high temperature) all the possible solutions are equiprobable, while once it go on, so the temperature go down, simulated annealing extract more frequently solution near the optimum. This means that the right solution become more probable at each iteration as it should naturally be and that the algorithm is working in a correct way.

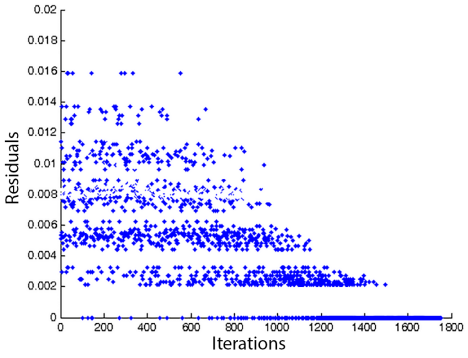

Figure 5.6: Residuals between observation and estimation of gravity data at each iteration of the solution algorithm

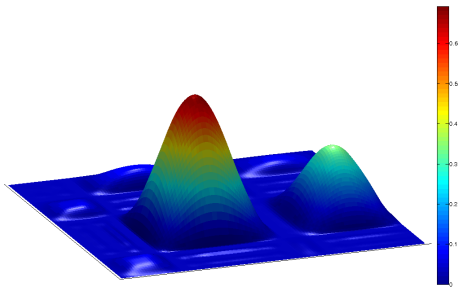

Figure 5.7: Example of posterior probability density function sampled for a single voxel

The other output obtained at the end of the iterative solution is the sampling of posterior probability density function of each voxel. An example is shown in figure 5.7, where the two planar axis are associated to the two used random variable. In particular for the current case there are three labels, each one with five values of density, discretized in the interval $\rho \pm 3\sigma_\rho$. The biggest pick is the most probable value for the considered voxel, while the smallest one is the second probable solution. This doesn't generate problem to the solution algorithm tanks to the characteristic of simulated annealing to find the global minimum of a solution, thus reaching the highest pick of *pdf* for each voxel.

Chapter 6

Conclusions and future work

In the present work a Bayesian approach to invert gravity data coupled with given geological prior models have been studied. The method works properly in the simple test done, improving the quality of solution if compared with traditional inversion solutions. In fact, the algorithm corrects between the 70% and 90% of the wrong voxels in geological prior knowledge. Actually, the main limiting factors are the computational time, the choice of the parameters in the formulation of a-posteriori probability, and the shape of the a-priory probabilities.

The computational time is very high, because in order to reach the convergence of the solution thousands of iteration are required. Moreover, in the test the synthetic models used have very low resolution, of the order of few kilometres. This level of accuracy in spatial description is useless in real gravity interpretation problems. In fact the required spatial resolution for practical application – i.e. Earth science, hydrocarbon exploration, etc. – is of the order of some hundreds of meters. That fact causes a huge increase of the total number of voxels: from some thousands to some millions, considering an investigated volume extension similar to that used in the test ($30 \times 30 \times 10\ km^3$). Actually, this portion of Earth subsurface is discretized using cube of dimension $1.5 \times 1.5 \times 1\ km^3$, thus the total quantity of voxels is 4000. In terms of unknown parameters the numbers is doubled, because of each voxel is associated to two variables: label and density. The number of unknown become 8000. If the resolution will be increased, and the volume is discretized using cube of dimension $100 \times 100 \times 100\ m^3$,considered realistic value in case of practical applications, the total number of voxels become 9 millions, thus the unknowns will be 18 millions. Clearly, this operation has deleterious effects on the computational time, that increase exponentially. Since this method is developed in order to invert airborne graviemtry data it is realistic consider a regular grid of observation of 2 $km \times 2\ km$, that cover 10 km apart from the borders of the investigate volume. The total number of collected observations is 400. This means that the forward matrix has dimension of $4000 \times 9 \cdot 10^6$. Obviously it's impossible to manage and store a similar quantity of data common PC. In order to allow the algorithm to run it's required the use of cluster computers, joined with strong optimized algorithm. Nowadays the only possible solution is to generate forward model using Fourier methods, that enhance appreciably the speed of computation.

As already seen increasing the spatial resolution implies an increase of the un-

known terms of the problem, thus leaving high variability and instability in the solution. To contain this two effects the parameters and weights present in the posterior probability density function must be accurately calibrated. In fact, they link all the terms in the posterior probability, in order to equalize the numerical difference due to the use of different measurement units and to reduce the dependence of the solution also from the total number of voxels and their dimensions. Actually, the user must set all this parameters by hand, thus losing lot of time in the fine calibration of the system. In the future, the aim is to develop a semi-automatic system able to determine weights and parameters, in order to limit as far as possible human decisions, and to speed up this calibration phase.

Furthermore, to stabilize the solution also some changing in the prior probability density function may be useful. In fact, now all the geological knowledge is considered given with a uniform and constant probability all over the investigated space. But, it is not unrealistic to think that this is not true and that some portions of the volume are known better than other. For example the knowledge derived from other geophysical inversion, like seismic, electrical, or magnetic prospections, with lower resolutions could be integrated. The outcome is the feasibility of a joint inversion Bayesian solution. Anyway, in order to give more information and to reach the convergence on a more stable solution future research and development must be oriented in the direction of that possibility of joint inversion, but also to study the possibility of integrate and use the information added by vector gravimetry or gravity gradiometry observation in this Bayesian approach.

The last focal point that is not fully treated in the present work is the convergence criteria. In fact, at the present the algorithm stop when an acceptable value of the residuals is reached, but in order to reduce the computational time a very useful trick could be to fix the unknowns when their posterior probability become greater than a fixed threshold (e.g. 95%). Using this kind of criteria every time that the two variables of a voxel are fixed they don't play more a role in the solution algorithm, thus reducing the time required for each iteration of simulated annealing. The software will be completed by a simple, but functional graphical user interface to allow data management and importation, parameters definition and results visualization. It will be useful to study which are the standards data format in geophysical prospecting technique, in order to maintain and implement them into the software.

Finally, the actual solution are done using simulated errorless data. That's why the development is in a preliminary phase and obviously it is only an ideal and not realistic condition. In fact, it should be studied how the observation errors influences the final results, because as seen in the examples the total signal amplitude is about $10 - 20$ $mGal$, and a realistic accuracy of the gravity observation is about $1 - 3$ $mGal$. This means that the signal has a relative precision about $10 - 20\%$ and the errors can play an important role in the final interpretation. Furthermore, it requires to be modelled, because specially in aero-gravimetry the noise cannot be considered white noise. In fact, due to signal preprocessing filtering of the signal the noise in the final observations is correlated between the various estimation point.

Bibliography

T.L. Abt, O. Huang, and C. Jekeli. Combination of local gravimetry and magnetic data to locate subsurface anomalies using a matched filter. In Steve Kenyon, Maria Christina Pacino, and Urs Marti, editors, *International Association of Geodesy Symposia, Proceedings of the 2009 IAG Symposium, Buenos Aires, Argentina, 31 August 31 - 4 September 2009: Geodesy for Planet Earth*, volume 136, pages 247–254. Springer Berlin Heidelberg, 2012.

R. Azencott. Simulated annealing. *Seminaire Bourbaki*, 30:223–237, 1988.

R. Barzaghi and F. Sansò. The integrated inverse gravimetric-tomographic problem: a continuous approach. *Inverse problems*, 14(3):499, 1998.

T. Bayes. An essay toward solving a problem in the doctrine of chances. *Philosophical Transactions of the Royal Society of London*, 53, 1984.

F.W. Bessel. Auszug aus einem Schreiben des Herrn Prof. Bessel. *Zach's Monatliche Correspondenz zur Beförderubng der Erd- un Himmelskunde, XXVII*, pages 80–50, 1813.

L. Biagi. *La stima della Moho mediante il metodo della collocazione*. PhD thesis, Università degli Studi di Modena, 1997.

L. Biagi and F. Sansò. Sistemi di riferimento in geodesia: algebra e geometria dei minimi quadrati per un modello con deficienza di rango: Parte prima. *Bollettino di geodesia e scienze affini*, 62(4):261–284, 2003.

L. Biagi and F. Sansò. Sistemi di riferimento in geodesia: algebra e geometria dei minimi quadrati per un modello con deficienza di rango parte seconda. *Bollettino di geodesia e scienze affini*, 63(1):29–52, 2004a.

L. Biagi and F. Sansò. Sistemi di riferimento in geodesia: algebra e geometria dei minimi quadrati per un modello con deficienza di rango parte terza. *Bollettino di geodesia e scienze affini*, 63(2):129–149, 2004b.

R.J. Blackely. *Potenntial Theory in Gravity and magnetic Applications*. Cambridge University Press, 1996.

M. Bosch. Lithologic tomography: from plural geophysical data to lithology estimation. *Journal of Geophysical Research: Solid Earth (1978–2012)*, 104(B1): 749–766, 1999.

G.E.P. Box and G.C. Tiao. *Bayesian inference in statistical analysis*, volume 40. John Wiley & Sons, 2011.

J.M. Brozena. A preliminary analysis of the NRL airborne gravimetry system. *Geophysics*, 49(7):1060–1069, 1984.

J.M. Brozena, G.L. Mader, and M.F. Peters. Interferometric Global Positioning System: Three-dimensional positioning source for airborne gravimetry. *Journal of Geophysical Research*, 94(B9):12153–12, 1989.

N.I. Christensen and W.D. Mooney. Seismic velocity structure and composition of the continental crust: A global view. *Journal of Geophysical Research: Solid Earth*, 100(B6):9761–9788, 1995. ISSN 2156-2202. doi: 10.1029/95JB00259.

C.E. Corbató. A least-squares procedure for gravity interpretation. *Geophysics*, 30 (2):228–233, 1965.

J. Czompo. *Airborne scalar gravimetry system errors in the spectral domain*. Geomatics Engineering, University of Calgary, 1994.

F.A. Darbyshire, R.S. White, and K.F. Priestley. Structure of the crust and uppermost mantle of iceland from a combined seismic and gravity study. *Earth and Planetary Science Letters*, 181(3):409 – 428, 2000. ISSN 0012-821X. doi: 10.1016/S0012-821X(00)00206-5.

M.C. De Lacy, F. Sansò, G. Rodriguez-Caderot, and A.J. Gil. The bayesian approach applied to gps ambiguity resolution. a mixture model for the discrete–real ambiguities alternative. *Journal of Geodesy*, 76(2):82–94, 2002.

C.V. Deutsch and A.G. Journel. *Geostatistical software library and user&s guide*, volume 1996. Oxford university press New York, 1992.

P. Dumrongchai. *Small Anomalous Mass Detection from Airborne Gradiometry*. Report 482. The Ohio State University, 2007.

ESA. http://www.esa.int/esa. Website. ESA official website.

M. Fedi and M.A. Abbas. A fast interpretation of self-potential data using the depth from extreme points method. *Geophysics*, 78(2):E107–E116, 2013.

M. Fedi and A. Rapolla. *I metodi gravimetrico e magnetico nella geofisica della Terra solida*. Liguori Editore, 1993. ISBN 9788820721015.

S. Geman and D. Geman. Stochastic relaxation, Gibbs distributions, and the Bayesian restoration of images. *Pattern Analysis and Machine Intelligence, IEEE Transactions on*, (6):721–741, 1984.

T. Grombein, K. Seitz, and B. Heck. Optimized formulas for the gravitational field of a tesseroid. *Journal of Geodesy*, pages 1–16, 2013.

I.B. Haáz. Relations between the potential of the attraction of the mass contained in a finite rectangular prism and its first and second derivatives. *Geophysical Transactions II*, 7:57–66, 1953.

J. Hadamard. Sur les problèmes aux dérivées partielles et leur signification physique. *Princeton University Bulletin*, pages 49–52, 1902.

J. Hadamard. Lectures on Cauchy's problem in linear partial differential equations. 1923.

S. Hammer. Airborne gravity is here! *Geophysics*, 48(2):213–223, 1983.

P.C. Hansen. The truncatedsvd as a method for regularization. *BIT Numerical Mathematics*, 27(4):534–553, 1987.

P.C. Hansen. *Rank-deficient and discrete ill-posed problems: numerical aspects of linear inversion*, volume 4. Siam, 1998.

B. Heck and K. Seitz. A comparison of the tesseroid, prism and point-mass approaches for mass reductions in gravity field modelling. *Journal of Geodesy*, 81 (2):121–136, 2007.

W.A. Heiskanen and H. Moritz. *Physical Geodesy*. Freeman, San Francisco, 1967.

G. Herglotz. Über das Benndorfsche Problem des Fortpflanzungsgeschwindigkeit der Erdbebenstrahlen. *Zeitschrift fúr Geophys*, 8:145–147, 1907.

B. Hofmann-Wellenhof and H. Moritz. *Physical geodesy*. Springer, 2006.

T. Ishihara. Gravimetric determination of the density of the Zenisu Ridge. *Tectonophysics*, 160(1):195–205, 1989.

D.D. Jackson and M. Matsu'ura. A Bayesian approach to nonlinear inversion. *Journal of Geophysical Research: Solid Earth (1978–2012)*, 90(B1):581–591, 1985.

C. Jekeli. Vector gravimetry using GPS in free-fall and in an earth-fixed frame. *Journal of Geodesy*, 66(1):54–61, 1992.

J.P. Kaipio and E. Somersalo. *Statistical and computational inverse problems*, volume 160. Springer, 2005.

P. Kearey, M. Brooks, and I. Hill. *An introduction to geophysical exploration*. Blackwell Science Ltd, 2009.

A. Kleusberg, D. Peyton, and D. Wells. Airborne gravimetry and the global positioning system. In *Position Location and Navigation Symposium, 1990. Record. The 1990's-A Decade of Excellence in the Navigation Sciences. IEEE PLANS'90., IEEE*, pages 273–278. IEEE, 1990.

E.T. Knickmeyer. Vector gravimetry by a combination of inertial and GPS satellite measurements. 1990.

L. LaCoste. The zero-length spring gravity meter. *The Leading Edge*, 7(7):20–21, 1988.

L. LaCoste, J. Ford, R. Bowles, and K. Archer. Gravity measurements in an airplane using state-of-the-art navigation and altimetry. *Geophysics*, 47(5):832–838, 1982.

A. Leick. *GPS satellite surveyng.* A Wiley - Interscience publication, 1995.

F.G. Lemoine, S.C. Kenyon, J.K. Factor, R.G. Trimmer, N.K. Pavlis, D.S. Chinn, C.M. Cox, S.M. Klosko, S.B. Luthcke, M.H. Torrence, et al. The development of the joint NASA, GSFC and the National Imagery and Mapping Agency (NIMA) geopotential model EGM96. 1998. *NASA Technical Report, NASA/TP-1998-206861.*

The Mathworks. http://www.mathworks.com/support/. Website. MatLab®support website.

H. Moritz. The figure of the Earth: theoretical geodesy and the Earth's interior. *Karlsruhe: Wichmann, c1990.*, 1, 1990.

K. Mosegaard and A. Tarantola. Monte Carlo sampling of solutions to inverse problems. *Journal of Geophysical Research*, 100(B7):12431–12, 1995.

K. Mosegaard and A. Tarantola. 16 probabilistic approach to inverse problems. *International Geophysics*, 81:237–265, 2002.

K. Mosegaard, S. Singh, D. Snyder, and H. Wagner. Monte Carlo analysis of seismic reflections from Moho and the W reflector. *Journal of geophysical research*, 102 (B2):2969–2981, 1997.

D. Nagy. The gravitational attraction of a rigth rectangular prism. *Geophysics XXXI*, pages 362–371, 1966.

D. Nagy, G. Papp, and J. Benedek. The gravitational potential and its derivatives for the prism. *Journal of Geodesy*, 74(7-8):552–560, 2000.

L.L. Nettleton, L. LaCoste, and J.C. Harrison. Tests of an airborne gravity meter. *Geophysics*, 25(1):181–202, 1960.

R.L. Parker. Best bounds on density and depth from gravity data. *Geophysics*, 39 (5):644–649, 1974.

R.L. Parker. The theory of ideal bodies for gravity interpretation. *Geophysical Journal International*, 42(2):315–334, 1975.

D.L. Phillips. A technique for the numerical solution of certain integral equations of the first kind. *Journal of the ACM (JACM)*, 9(1):84–97, 1962.

D. Plouff. Gravity and magnetic field of polygonal prisms and application to magnetic terrain correction. *Geophysics*, 41:727–741, 1976.

F. Press. Earth models obtained by Monte Carlo inversion. *Journal of Geophysical Research*, 73(16):5223–5234, 1968.

J.M. Reynolds. *An introduction to applied and environmental geophysic*. John Wiley and sons, 1997.

Y.A. Rozanov. *Markov random fields*. Springer, 1982.

O.S. Salychev. *Inertial surveying: ITC Ltd. experience*. MSTU Press, 1995.

O.S. Salychev, A.V. Bykovsky, V.V. Voronov, K.P. Schwarz, Z. Liu, M. Wei, and J. Paneka. Determination of gravity and deflections of the vertical for geophysical applications using the ITC-2 platform. In *Proceedings, International Symposium on Kinematic Systems in Geodesy, Geodynamics and Navigation, University of Calgary*, pages 521–529, 1994.

D. Sampietro and F. Sansó. Uniqueness theorems for inverse gravimetric problems. In Nico Sneeuw, Pavel Novák, Mattia Crespi, and Fernando Sansò, editors, *International Association of Geodesy Symposia, "VII Hotine-Marussi Symposium on Mathematical Geodesy", 6 - 10 June 2009, Rome, Italy*, volume 137, pages 111–115. Springer Berlin Heidelberg, 2012.

F. Sansò, M. Reguzzoni, and D. Triglione. *Metodi Monte Carlo e delle Catene di Markov: una itnroduzione*. Maggioli Editore, 2011.

F. Sansò and M.G. Sideris. *Geoid Determination: Theory and Methods*. Lecture Notes in Earth System Sciences. Springer, 2012. ISBN 9783540746997.

K.P. Schwarz and Y.C. Li. What can airborne gravimetry contribute to geoid determination? *Journal of Geophysical Research: Solid Earth (1978–2012)*, 101(B8): 17873–17881, 1996.

K.P. Schwarz and Z. Li. An introduction to airborne gravimetry and its boundary value problems. In *Geodetic boundary value problems in view of the one centimeter geoid*, pages 312–358. Springer, 1997.

K.P. Schwarz, M.E. Cannon, and R.V.C. Wong. A comparison of GPS kinematic models for the determination of position and velocity along a trajectory. *Manuscripta geodaetica*, 14(2):345–353, 1989.

K.P. Schwarz, O. Colombo, G. Hein, and E.T. Knickmeyer. Requirements for airborne vector gravimetry. In *From Mars to Greenland: Charting Gravity With Space and Airborne Instruments*, pages 273–283. Springer, 1992.

A. Tarantola. *Inverse problem theory: Methods for data fitting and model parameter estimation*. Elsevier Science, 2002.

A. Tarantola and B. Valette. Inverse problems = quest for information. *J. geophys*, 50(3):150–170, 1982.

L.G.D. Thompson. Airborne gravity meter test. *Journal of Geophysical Research*, 64(4):488–488, 1959.

L.G.D. Thompson and L.J.B. LaCoste. Aerial gravity measurements. *Journal of Geophysical Research*, 65(1):305–322, 1960.

A.N. Tikhonov. Solution of incorrectly formulated problems and the regularization method. *Soviet Math Dokl*, 4:1035–1038, 1963.

I. Todhunter. *A History of the Mathematical Theories of Attraction and the Figure of the Earth from the Time of Newton to that of Laplace*, volume 1. Macmillan, 1873.

S. Twomey. On the numerical solution of Fredholm integral equations of the first kind by the inversion of the linear system produced by quadrature. *Journal of the ACM (JACM)*, 10(1):97–101, 1963.

L. Uieda. *Tesseroids Documentation. Release 1.1-beta*. 2013.

M. Wei and K.P. Schwarz. Flight test results from a strapdown airborne gravity system. *Journal of Geodesy*, 72(6):323–332, 1998.

M. Wei, S. Ferguson, and K.P. Schwarz. Accuracy of gps-derived acceleration from moving platform tests. In *From Mars to Greenland: Charting Gravity With Space and Airborne Instruments*, pages 235–249. Springer, 1992.

R.A. Wiggins. Monte Carlo inversion of body-wave observations. *Journal of Geophysical Research*, 74(12):3171–3181, 1969.